1991

Zeeman mixing in 6(2)P rubidium atoms induced in noble-gas collisions.

R. Blair. Middleton
University of Windsor

NOTICE

The quality of this microform is heavily dependent upon the quality of the original thesis submitted for microfilming. Every effort has been made to ensure the highest quality of reproduction possible.

If pages are missing, contact the university which granted the degree.

Some pages may have indistinct print especially if the original pages were typed with a poor typewriter ribbon or if the university sent us an inferior photocopy.

Reproduction in full or in part of this microform is governed by the Canadian Copyright Act, R.S.C. 1970, c. C-30, and subsequent amendments.

AVIS

La qualité de cette microforme dépend grandement de la qualité de la thèse soumise au microfilmage. Nous avons tout fait pour assurer une qualité supérieure de reproduction.

S'il manque des pages, veuillez communiquer avec l'université qui a conféré le grade.

La qualité d'impression de certaines pages peut laisser à désirer, surtout si les pages originales ont été dactylographiées à l'aide d'un ruban usé ou si l'université nous a fait parvenir une photocopie de qualité inférieure.

La reproduction, même partielle, de cette microforme est soumise à la Loi canadienne sur le droit d'auteur, SRC 1970, c. C-30, et ses amendements subséquents.

ZEEMAN MIXING IN 6^2P RUBIDIUM ATOMS INDUCED IN NOBLE-GAS COLLISIONS

By

R. Blair Middleton

A Thesis
Submitted to the Faculty of Graduate Studies and Research
through the Department of Physics in
Partial Fulfillment of the Requirements for the
Degree of Master of Science at the
University of Windsor

Windsor, Ontario, Canada
1991

ISBN 0-315-65139-3

Abstract

Rubidium vapour, together with a noble gas contained in a cell located in a 4.75T magnetic field, was irradiated with light from a pulsed dye laser. This radiation produced selective excitation of the $6^2P_{J,m}$ (J=1/2,3/2, m=-3/2,-1/2,1/2,3/2) Zeeman substates. Collisions of the excited 6P atoms with He, Ne and Ar atoms and the resulting Zeeman mixing produced a population in the whole 6P Zeeman manifold and resulted in the emission of a Zeeman fluorescence spectrum which was resolved with a scanning Fabry-Perot interferometer, detected with a photomultiplier and stored in a multichannel scaler. The analysis of the fluorescence intensities of the components emitted in the decay of the directly (optically) excited state and of the collisionally populated states in relation to the noble gas densities, yielded the Zeeman mixing cross sections and the cross sections for the relaxation of dipole, quadrupole, and octupole moments.

I would like to dedicate this thesis to Miss Hazel Goy, for standing beside me for so long and whose love and support has made my work so much easier.

Acknowledgements

I am most grateful to my supervisor, Dr. L. Krause, for his assistance and support of this work and in particular for his corrections while reading this thesis in manuscript. I should like to express my most sincere thanks to Dr. W. Kedzierski for his invaluable advice and suggestions during the course of this work and to Dr. R. Berends for his assistance and advice at the beginning of this project. I am also grateful to the faculty, staff and fellow graduate students for creating a helpful climate in which to work of which, Dr. J. B. Atkinson deserves special attention for his advice with working out the computer related problems during the course of this investigation.

Acknowledgements are due to Mr. B. Masse, Mr. S. Gillen and Mr. P. Seguin in the electronics shop, Mr. W. Grewe in the machine shop and Mr. A. Ditchburn the glass blower, for their assistance in the maintenance and upgrading of the equipment in this investigation, and to Mr. R. Buzzeo for his skill in the preparation of some of the diagrams which appear in this dissertation.

I would also like to express my most sincere thanks to my parents, Robert and Helen Middleton, for their love and support throughout my university career and to my girlfriend, Hazel Goy, for her assistance in the typing and preparation of this manuscript.

Table of Contents

List of Tables

List of Figures

1. Introduction

Experimental measurements and theoretical calculations of inelastic collisional interactions of excited atoms with ground state atoms and molecules have provided useful information in a variety of fundamental scientific areas such as atomic physics and astrophysics. The physical behavior of such systems as stellar atmospheres or the upper atmosphere, where atoms and molecules are continuously excited and de-excited by the absorption and re-emission of radiation and by collisions with other bodies, is determined by their relaxation rates and cross sections. The understanding of the processes of collisional transfer allows the development of theoretical models which can describe and sometimes predict some experimental observations. Collisions involving alkali metals are of special interest due to their relatively simple hydrogen-like atomic structure which lends itself to easier theoretical modeling, and their relatively low melting point which makes possible their easy investigation in the laboratory.

When an alkali vapour contained in a cell is irradiated with one fine-structure (fs) component of the resonance radiation, inelastic collisions of the excited atoms with the ground state atoms cause the population of the other fs state whose decay results in the emission of sensitized fluorescence in addition to the resonance fluorescence emitted from the primarily populated state. Wood and his associates (1918) carried out the first investigation of sensitized fluorescence in a sodium-argon system. Their studies of excitation transfer were fol-

lowed by similar experiments of Lochte-Holtgreven (1928), Thangaraj (1948), Seiwert (1956), and Jordan (1964) who studied various alkali-noble gas mixtures. These experiments were generally performed at high vapour and gas pressures, where the measurements were subject to considerable error arising from radiation diffusion, quenching and pressure broadening. This and some subsequent work is described in a review article by Krause (1975).

In 1922, Wood discovered the pressure broadening of the Hg resonance line and found that the addition of a buffer gas to the fluorescing system destroyed the observed polarization of the fluorescence. The selective excitation of a particular atomic state may create a non-equilibrium population and specifically, the selective optical excitation of a Zeeman substate results in the polarization of the gas or vapour. This polarization manifests itself through detectable changes in the fluorescence. Some of the first reported experiments utilizing the depolarization of the fluorescence to study the relaxation cross sections from interactions of atoms with noble gases in high magnetic-fields were by Berdowski et al. (1971) for potassium and by Seiwert (1956) and Gay and Schneider (1976) for sodium. An atomic vapour is said to be polarized if a non-equilibrium population distribution exists among the Zeeman substates. Collisions between the excited alkali-metal atoms and the noble gas atoms in their ground state, tend to equalize the Zeeman populations and cause relaxation of the atomic multipoles accompanied by the depolarization of the fluorescence. The study of this depolarization or of changes in the excited state Zeeman population dis-

tribution in relation to the density of the ground-state atoms inducing the relaxation leads to the cross sections for m_J mixing or multipole relaxation (Baylis 1979). The depolarization of the $^2P_{1/2}$ state results from its dipole relaxation while the depolarization of the $^2P_{3/2}$ state results from the relaxation of its dipole, quadrupole and octupole moments. The rates or cross sections for circular depolarization (also called disorientation) or linear depolarization (disalignment), provide an insight into the details of the collisional interactions between the excited atoms and the ground state atoms of the buffer gas. Collisional depolarization is extensively discussed in review articles of Baylis (1979) and Elbel (1979).

More recently, Spielfiedel *et al.* (1979) calculated the relaxation cross sections of the K(5P) state using both semi-classical and quantum techniques. Pascale (1987) calculated the Zeeman mixing cross sections for collisions of K(5P) atoms with He. Baylis (1979) outlined a general matrix formulation for computing collisional depolarization and the resulting cross sections. Pascale and Vandeplanque (1974) calculated various interatomic model potentials for thermal collisions between an alkali and noble gas atom and depolarization cross sections were calculated by Rebentrost *et al.* (1987) for resonance state alkali-metals in interactions with He atoms. Guiry and Krause (1972) studied experimentally the cross sections for disorientation of Cs(6P) atoms in a magnetic field of 0.98T. Skalinski and Krause (1982) and Boggy and Franz (1982) studied the relaxation of the K(4P) atoms in collision with ground-state potassium and noble-gas atoms in magnetic fields up to 1T,

and Berends et al. (1988) determined the multipole relaxation cross sections for K(5P) in collision with He, Ne and Ar atoms at a magnetic field of 7T.

In this experiment, the individual Rb (6^2P <-> 5^2S) Zeeman components were resolved in excitation and emission, which took place in Rb-noble gas mixtures. This mixture was placed in a relatively strong magnetic field, thus the electronic and nuclear moments in the rubidium atoms were effectively decoupled from each other and the measured cross sections were not affected by the "flywheel" effect" of the nucleus (Bulos and Happer 1971). The relative intensities of the Zeeman fluorescence components were determined in relation to the buffer gas densities and the experimental data yielded the cross sections for mixing among the various 6^2P m_J states. The fine-structure mixing and multipole relaxation cross sections were obtained from the m_J mixing cross sections. This thesis describes the first experimental determination of the multipole relaxation cross sections for collisions of Rb(6P) atoms with He, Ne and Ar in a high magnetic field (4.75 T). A partial Grotrian diagram for rubidium is shown in Fig 1.1 and the relative displacements of the 6P Zeeman substates of rubidium for a magnetic field of 4.75 T are shown in Fig A.1, in Appendix A.

Fig 1.1 Partial Grotrian Diagram for Rb.

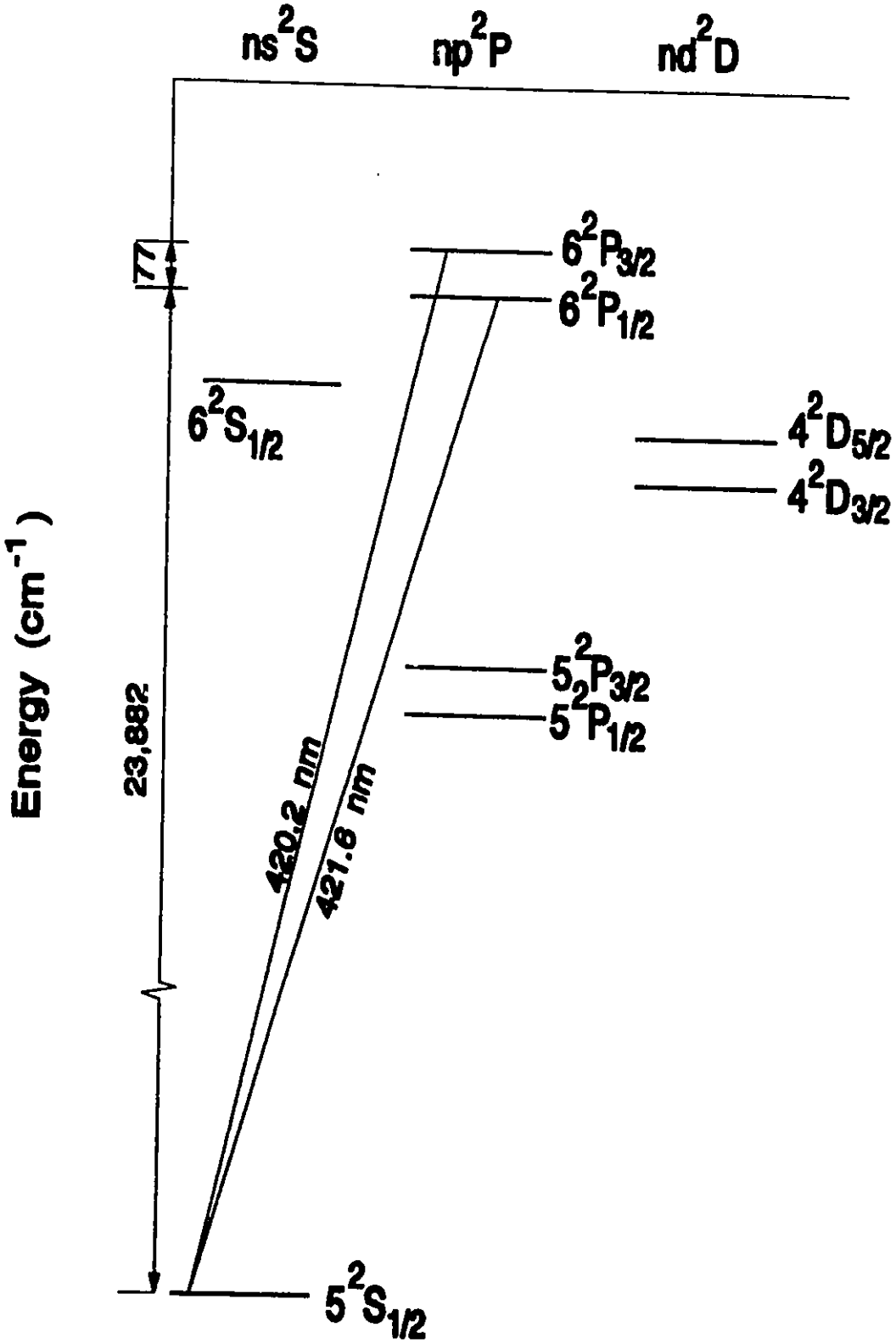
ns²S
np²P
nd²D
Energy (cm⁻¹)
77
23,882
6²P3/2
6²P1/2
6²S1/2
4²D5/2
4²D3/2
5²P3/2
5²P1/2
420.2 nm
421.8 nm
5²S1/2

2. Theoretical

2.1 Selective Excitation and Decay of the Rb 6^2P Zeeman Sublevels

The selective optical excitation of a particular atomic Zeeman sublevel may create a non-equilibrium population distribution among the Zeeman substates within an ensemble of atoms in an alkali vapour. The selective optical excitation of a Zeeman sublevel also results in the polarization of the vapour, which manifests itself by the polarization of the emitted fluorescence. This polarization may be described as the creation of a bulk magnetic multipole moment in the vapour (Baylis 1978).

When Rb atoms are excited to a 6P Zeeman sublevel in a mixture of Rb vapour with a noble gas, collisional interactions between the polarized Rb atoms and the noble gas atoms cause the redistribution of population through collisional excitation transfer to the other Zeeman substates within the 6^2P manifold. This transfer results in the depolarization of the resulting fluorescence and the collisional relaxation of the multipole moments, and may be described in terms of rates or cross sections for the relaxation of the multipole moments. The depolarization of a $^2P_{1/2}$ state is described by the relaxation of the dipole moment (disorientation), while the depolarization of a $^2P_{3/2}$ state involves the relaxation of dipole, quadrupole (disalignment) and octupole moments.

The polarization of the fluorescence can be monitored in terms of intensities of the linearly and circularly polarized components. The degrees of polarizations may be determined experimentally by using the relations:

$$P_{CIRC} = \frac{I_{\sigma^-} - I_{\sigma^+}}{I_{\sigma^-} + I_{\sigma^+}} \qquad 2.1.1$$

$$P_{LIN} = \frac{I_{\pi} - I_{\sigma}}{I_{\pi} + I_{\sigma}} \qquad 2.1.2$$

where I_{σ} and I_{π} are the relative intensities of the respective σ and π fluorescence components emitted perpendicularly to the field, and I_{σ^+}, I_{σ^-} are the intensities of the σ^+ and σ^- components emitted parallel to the field. The spontaneous decay of the excited Zeeman substates results in linearly polarized π radiation emitted perpendicular to the magnetic field and circularly polarized σ radiation emitted parallel to the field. It is possible to study the collisional relaxation of the dipole and quadrupole moments associated with excited 6^2P Rb atoms by determining the degrees of circular and linear polarization, respectively, in relation to the buffer gas pressures. In order, however, to determine the cross sections for the relaxation of the octupole (and higher) moments, it is not sufficient to determine the degrees of polarization but the fluorescence must also be spectrally resolved, to allow the determination of the relative intensities of all the Zeeman components present in the fluorescence.

In this experiment, only circularly polarized fluorescence was detected, and the measured integrated intensities of the fluorescence components may be expressed by:

$$\frac{N_{J,m}}{N_{J',m'}} = \frac{I_{J,m}}{I_{J',m'}} \frac{A^{\sigma}_{J',m'}}{A^{\sigma}_{J,m}} \qquad 2.1.3$$

where $N_{J,m}$ are the population densities of the Zeeman substates and $A^{\sigma}_{J,m}$ are the appropriate Einstein A coefficients for decay of the excited states by emission of circularly polarized light (Mitchell and Zemansky 1934). These Einstein A coefficients are magnetic field-dependent.

For the $6^2P_{\frac{1}{2}} \rightarrow 5^2S_{\frac{1}{2}}$ and $6^2P_{\frac{3}{2}} \rightarrow 5^2S_{\frac{1}{2}}$ transitions in zero magnetic field, the ratios of the Einstein A coefficients for the emission of polarized radiation are:

$$A^{\pi}_{\frac{1}{2}\leftrightarrow\frac{1}{2}} : A^{\sigma}_{\frac{1}{2}\leftrightarrow\frac{1}{2}} = 1:2$$

2.1.4

$$A^{\sigma}_{\frac{3}{2}\leftrightarrow\frac{3}{2}} : A^{\sigma}_{\frac{3}{2}\leftrightarrow\frac{1}{2}} : A^{\pi}_{\frac{1}{2}\leftrightarrow\frac{1}{2}} = 3:1:2$$

Since the oscillator strengths for the $6P^2_{1/2} \rightarrow 5S^2_{1/2}$ and $6P^2_{3/2} \rightarrow 5S^2_{1/2}$ transitions are very nearly equal to one another (Migdalek and Baylis 1979), eq. (2.1.4) may be expressed in terms of emission of circularly polarized light components (Boggy and Franz 1982):

$$A^{\sigma}_{\frac{3}{2}\leftrightarrow\frac{3}{2}} : A^{\sigma}_{\frac{3}{2}\leftrightarrow\frac{1}{2}} : A^{\sigma}_{\frac{1}{2}\leftrightarrow\frac{1}{2}} = 3:1:2 \qquad 2.1.5$$

These A coefficients (which give the transition probability of spontaneous emission) must be described so that they take into account the perturbation effects on the wave functions resulting in increased mixing between the Zeeman substates, due to the high magnetic field (Boggy and Franz 1982). In a magnetic field B = 4.75T, the A coefficients are in the ratio:

$$\begin{aligned} & A^{q}_{\frac{3}{2}^{*}\frac{3}{2}}(B) : A^{q}_{\frac{3}{2}^{*}\frac{1}{2}}(B) : A^{q}_{\frac{1}{2}^{*}\frac{1}{2}}(B) \\ &= 3 : 1 - \frac{2\sqrt{2}\mu_B B}{3\Delta E} : 2 - \frac{\sqrt{2}\mu_B B}{2\Delta E} \\ &= 3.00 \ : \ 0.97 \ : \ 2.01 \end{aligned} \qquad 2.1.6$$

where μ_B is the Bohr magneton and $\Delta E = 77.38 cm^{-1}$.

2.2 Collisional m_J Mixing

Collisions with the ground-state noble gas or rubidium atoms tend to equalize the Zeeman state populations:

$$Rb(6^2P_{J,m}) + X \rightarrow Rb(6^2P_{J',m'}) + X + \Delta E' \qquad 2.2.1$$

where X is the buffer gas atom, $\Delta E'$ is the change in kinetic energy of the collision partners, J or $J' = \frac{1}{2}, \frac{3}{2}$ and m or $m' = \frac{3}{2}, \frac{1}{2}, -\frac{1}{2}, -\frac{3}{2}$.

Continuous optical excitation results in a steady state which involves excitation, spontaneous decay to the ground state and collisional transfer between Zeeman substates. The following rate equation represents these processes (Skalinski and Krause 1982):

$$\frac{dN_{J,m}}{dt} = -\frac{N_{J,m}}{\tau} - N_{J,m}\sum_{m'\neq m} Z(m \rightarrow m') + \sum_{m'\neq m} N_{J,m'} Z(m \leftarrow m') + S_{J,m} = 0 \qquad 2.2.2$$

where Z is the frequency of Zeeman mixing collisions per excited atom. $Z = Q\upsilon$ where Q is the cross section associated with a particular Zeeman mixing process and υ is the average relative speed of the colliding atoms.

$$\upsilon = \left(\frac{8kT}{\pi\mu}\right)^{\frac{1}{2}} \qquad 2.2.3$$

where k is the Boltzmann constant, T is the temperature of the fluorescing vapour-gas mixture and μ is the reduced mass of the colliding pair. $N_{J,m}$ is the population density of the Zeeman substates and $S_{J,m}$ is the density of atoms excited per second to state m. The mean radiative lifetime, τ, of the 6^2P state is taken to be $11.5\times10^{-8}s$ which is the average of $\tau_{\frac{1}{2}} = 11.68\times10^{-8}s$ (Gallagher 1969) and $\tau_{\frac{3}{2}} = 11.4\times10^{-8}s$ (Bucka et al. 1966). Eq. (2.2.2) may also be stated in the density matrix formalism (Baylis 1979):

$$\dot{\vec{N}} = \vec{S} - \hat{\Gamma}\vec{N} - \hat{\gamma}\vec{N} \qquad 2.2.4$$

where $\vec{N}$ = population density vector, $\vec{S}$ represents the optical excitation rate of the Zeeman states, $\hat{\Gamma}$ is the matrix describing the spontaneous decay rate of the excited state to the ground state and $\hat{\gamma}$ is the matrix describing the rate of collisional transfer between all the Zeeman sublevels in the manifold.

The Zeeman mixing cross section may be defined analogously with the gas-kinetic cross section:

$$\gamma(J,m\rightarrow J',m') = N\upsilon Q(J,m\rightarrow J',m') \qquad 2.2.5$$

where $\gamma(J,m\rightarrow J',m')$ represents the rate of transfer between the Zeeman substates of the 6^2P manifold and N is the density of the buffer gas atoms. Under single-collision conditions, when an excited Rb atom undergoes at most one inelastic collision during its lifetime (Berends, et al. 1989):

$$N\upsilon Q(J,m\rightarrow J',m') \ll \tau^{-1} \qquad 2.2.6$$

Equations (2.2.1) and (2.2.2) assume that there will be only an insignificant amount of collisional quenching to the ground state.

The Zeeman mixing cross sections follow from equations (2.2.5) and (2.2.6):

$$Q(J,m\rightarrow J',m') = (1/N\upsilon\tau)(N_{J',m'}/N_{J,m}) \qquad 2.2.7$$

The multipole relaxation cross sections $\Lambda^{(L)}_{1/2}$ and $\Lambda^{(L)}_{3/2}$ (L = 1,2,3) are related as follows to calculated the Zeeman mixing cross sections $Q(J,m\rightarrow J',m')$ (Baylis 1979):

$$\Lambda^{(1)}_{\frac{1}{2}} = 2Q\left(\frac{1}{2}-\frac{1}{2}\rightarrow\frac{1}{2}\frac{1}{2}\right) \qquad 2.2.8$$

$$\Lambda^{(1)}_{\frac{3}{2}} = 2Q\left(\frac{3}{2}-\frac{3}{2}\rightarrow\frac{3}{2}\frac{3}{2}\right)+\frac{4}{3}Q\left(\frac{3}{2}-\frac{3}{2}\rightarrow\frac{3}{2}\frac{1}{2}\right)+\frac{2}{3}Q\left(\frac{3}{2}-\frac{3}{2}\rightarrow\frac{3}{2}-\frac{1}{2}\right) \qquad 2.2.9$$

$$\Lambda^{(2)}_{\frac{3}{2}} = 2Q\left(\frac{3}{2}-\frac{3}{2}\rightarrow\frac{3}{2}\frac{1}{2}\right)+2Q\left(\frac{3}{2}-\frac{3}{2}\rightarrow\frac{3}{2}-\frac{1}{2}\right) \qquad 2.2.10$$

$$\Lambda^{(3)}_{\frac{3}{2}} = 2Q\left(\frac{3}{2}-\frac{3}{2}\rightarrow\frac{3}{2}\frac{3}{2}\right)-2Q\left(\frac{3}{2}-\frac{3}{2}\rightarrow\frac{3}{2}\frac{1}{2}\right)+4Q\left(\frac{3}{2}-\frac{3}{2}\rightarrow\frac{3}{2}-\frac{1}{2}\right) \qquad 2.2.11$$

Because the Zeeman splitting is much smaller than kT $(kT = 269cm^{-1})$,

$$Q(J, m \to J', m') = Q(J, -m \to J', -m') \qquad 2.2.12$$

Berdowski et al. (1971) and Boggy and Franz (1982) derived additional transformation equations with the aid of eq. (2.2.12):

$$\Lambda_{\frac{1}{2}}^{(1)} = 2Q\left(\frac{1}{2}\frac{1}{2} \to \frac{1}{2} - \frac{1}{2}\right) \qquad 2.2.13$$

$$\Lambda_{\frac{3}{2}}^{(1)} = \frac{1}{5}Q\left(\frac{3}{2} - \frac{1}{2} \to \frac{3}{2}\frac{1}{2}\right) + \frac{8}{5}Q\left(\frac{3}{2} - \frac{3}{2} \to \frac{3}{2}\frac{1}{2}\right) + \frac{9}{5}Q\left(\frac{3}{2} - \frac{3}{2} \to \frac{3}{2}\frac{3}{2}\right) + \frac{2}{5}Q\left(\frac{3}{2}\frac{3}{2} \to \frac{3}{2}\frac{1}{2}\right) \qquad 2.2.14$$

$$\Lambda_{\frac{3}{2}}^{(2)} = 2Q\left(\frac{3}{2} - \frac{3}{2} \to \frac{3}{2}\frac{1}{2}\right) + 2Q\left(\frac{3}{2}\frac{3}{2} \to \frac{3}{2}\frac{1}{2}\right) \qquad 2.2.15$$

$$\Lambda_{\frac{3}{2}}^{(3)} = \frac{9}{5}Q\left(\frac{3}{2} - \frac{1}{2} \to \frac{3}{2}\frac{1}{2}\right) + \frac{2}{5}Q\left(\frac{3}{2} - \frac{3}{2} \to \frac{3}{2}\frac{1}{2}\right) + \frac{1}{5}Q\left(\frac{3}{2} - \frac{3}{2} \to \frac{3}{2}\frac{3}{2}\right) + \frac{8}{5}Q\left(\frac{3}{2}\frac{3}{2} \to \frac{3}{2}\frac{1}{2}\right) \qquad 2.2.16$$

The multipole relaxation cross sections $\Lambda_{11}^{(L)}$ and $\Lambda_{22}^{(L)}$ $(L = 1,2,3)$ are defined by Baylis (1979) and Elbel (1979):

$$\sigma_{11}^{(L)} = \sigma_{11}^{(0)} + \Lambda_{11}^{(L)} \quad ; \quad \sigma_{22}^{(L)} = \sigma_{22}^{(0)} + \Lambda_{22}^{(L)} \qquad 2.2.17$$

Accordingly the fine-structure mixing cross sections, $\sigma^{(0)}$ and orientation-transfer cross sections, $\sigma^{(1)}$ are:

$$\gamma_{ij}^{(0)}(J \to J') = Nv\sigma^{(0)}(J \to J') \qquad 2.2.18$$

$$-\gamma_{ij}^{(1)}(J \to J') = Nv\sigma^{(1)}(J \to J') \qquad 2.2.19$$

with the arrow indicating the direction of transfer. $\sigma_{12}^{(0)}$ and $\sigma_{21}^{(0)}$ are defined as:

$$\sigma_{12}^{(0)}\left(\frac{1}{2}\rightarrow\frac{3}{2}\right) = \frac{1}{\sqrt{2}}\sigma_{11}^{0} \qquad 2.2.20$$

$$\sigma_{21}^{(0)}\left(\frac{3}{2}\rightarrow\frac{1}{2}\right) = \sqrt{2}\sigma_{22}^{0} \qquad 2.2.21$$

and these are all related to the corresponding Zeeman mixing cross sections by:

$$\sigma_{21}^{(0)} = \frac{1}{\sqrt{2}}\sum_{m} Q\left(\frac{1}{2},-\frac{1}{2}\rightarrow\frac{3}{2},m\right) \qquad 2.2.22$$

$$\sigma_{12}^{(0)} = \sqrt{2}\left(Q\left(\frac{3}{2},-\frac{3}{2}\rightarrow\frac{1}{2},-\frac{1}{2}\right)+Q\left(\frac{3}{2},-\frac{3}{2}\rightarrow\frac{1}{2},\frac{1}{2}\right)\right) \qquad 2.2.23$$

$$\sigma_{21}^{(1)} = \frac{1}{\sqrt{10}}\left(3Q\left(\frac{1}{2}-\frac{1}{2}\rightarrow\frac{3}{2}-\frac{3}{2}\right)+Q\left(\frac{1}{2}-\frac{1}{2}\rightarrow\frac{3}{2}-\frac{1}{2}\right)\right.$$
$$\left.-Q\left(\frac{1}{2}-\frac{1}{2}\rightarrow\frac{3}{2}\frac{1}{2}\right)-3Q\left(\frac{1}{2}-\frac{1}{2}\rightarrow\frac{3}{2}\frac{3}{2}\right)\right) \qquad 2.2.24$$

$$\sigma_{12}^{(1)} = \frac{\sqrt{10}}{3}\left(Q\left(\frac{3}{2}-\frac{3}{2}\rightarrow\frac{1}{2}-\frac{1}{2}\right)-Q\left(\frac{3}{2}-\frac{3}{2}\rightarrow\frac{1}{2}\frac{1}{2}\right)\right) \qquad 2.2.25$$

$\gamma_{11}^{(0)} = N v \sigma_{11}^{(0)}$ and $\gamma_{22}^{(0)} = N v \sigma_{22}^{(0)}$ are the depopulation rates for the $6^2P_{1/2}$ and $6^2P_{3/2}$ states, respectively, with the fs orientation transfer rates defined by : $\gamma_{12}^{(1)} = N v \sigma_{12}^{(1)}$ and $\gamma_{21}^{(1)} = -N v \sigma_{21}^{(1)}$. Since the fs transfer cross sections measured in the absence of a magnetic field are equivalent to the depopulation cross sections $\sigma_{11}^{(0)}$ and $\sigma_{22}^{(0)}$ (Berends 1988):

$$Q_{12} = \sigma_{11}^{(0)} \qquad 2.2.26$$

$$Q_{21} = \sigma_{22}^{(0)} \qquad 2.2.27$$

3 The Apparatus and Experimental Procedure

3.1 General Description of the Apparatus

The arrangement of the apparatus is shown schematically in Fig. (3.1.1). Radiation from a N_2-laser-pumped dye laser was made incident on Rb vapour contained in a quartz fluorescence cell, to selectively excite all the 6P Zeeman states in turn. The cell also contained variable pressures of a noble gas and was placed in a uniform 4.75-T magnetic field. The resulting fluorescence pulses from the vapour-gas mixture were monitored at right angles to the direction of excitation and parallel to the magnetic field. The fluorescence spectrum consisted of a direct component emitted in the decay of the optically populated m_J substate, and sensitized fluorescence components, emitted from the Zeeman substates populated by collisions. The spectrum was resolved with a scanning Fabry-Perot interferometer and detected with a photomultiplier whose output was buffered into a pulse sampler. These data were subsequently accumulated in a multichannel scaler (MCS), and were transferred to a microcomputer for further analysis.

Fig 3.1.1 Schematic diagram of the apparatus. Amp, amplifier discriminator; B, applied magnetic field; Das10, stabilizer controller; DB, delay box; DL, dye laser; F, filter; FC, fibre optic cable; FP, Fabry-Perot interferometer; Gate, gated pulse-inverter amplifier; HeNe L, HeNe laser; LT, channel advance laser trigger; MCS, multichannel scaler; N_2L, nitrogen gas laser; PC, computer; PD, photodiode; PS, pulse sampler; Ramp, ramp signal generator; S1, S2, shutters; SC, shutter controller; T, telescope.

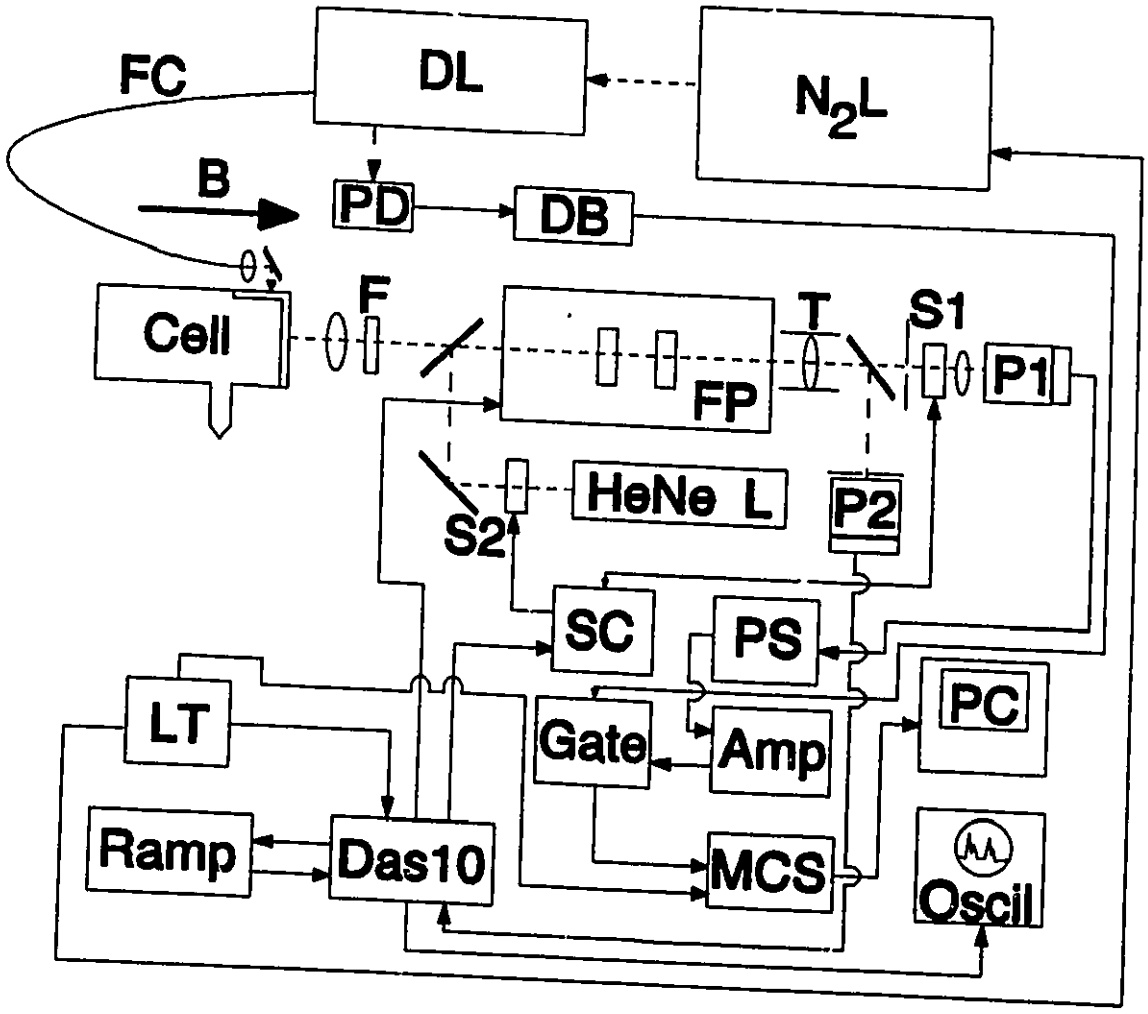
FC
DL
N2L
B
PD
DB
Cell
F
T
S1
FP
P1
HeNe L
P2
S2
SC
PS
LT
Gate
Amp
PC
Ramp
Das10
MCS
Oscil

3.2 The Fluorescence Cell and Gas-Filling System

The rectangular quartz fluorescence cell had dimensions 2.5x2.5x4.0 cm and was fitted with a small side-arm which protruded downwards and contained an excess of rubidium. The entire cell was enclosed in a cylindrical oven heated by silicon oil circulated by a Neslab ultrathermostat. The side-arm had a separate heating unit and was kept approximately 40°C below the rest of the cell. This controlled the Rb vapour pressure in the cell whose temperature was monitored by three copper-constantan thermocouples placed at various points on the cell. The whole oven was placed in the bore of the superconducting magnet. The cell was connected to a vacuum and gas filling system by means of a Teflon stopcock. The buffer gasses were admitted into the cell as required.

The vacuum and gas filling system included an Edwards E02 two-inch, oil diffusion pump fitted with a liquid nitrogen cold trap and backed up with a Edwards E2M2 mechanical roughing pump. The oil diffusion pump used Santovac 5 oil and produced an ultimate vacuum of 5×10^{-8} Torr. The system included flasks of research grade He, Ne and Ar gases (supplied by the Matheson Company[1]). The gases were admitted into the cell as needed and their pressures were monitored with a Granville-Phillips (model 275) Convectron gauge.

---

1 Minimum gas purity rated at 99.9995%

Before beginning the experiments, the fluorescence cell was charged with re-distilled rubidium metal, pumped down to $8x10^{-8}$ Torr, and isolated from the rest of the vacuum system. The heating elements were first adjusted to hold the side-arm approximately 80°C below the temperature of the cell (held at 115°C), to ensure no condensation of rubidium on the cell windows. The cell was then flushed with the noble gas and the side-arm temperature was increased to 40°C below the main cell temperature. The noble gas was then pumped out of the system and replaced with the appropriate quantity needed to begin the experiment. After the required fluorescence signal was recorded, the gas pressure was then lowered by pumping out the cell and re-filling it with a lower amount of buffer-gas. This procedure of pumping the cell down and isolating it was repeated before each different noble-gas was used. The side-arm temperature was held at 75°C, which resulted in an acceptable signal-to-noise ratio and a vapour pressure approximately of $3x10^{-5}$ Torr.

The buffer gases were kept in the cell for not longer than 6 hours and the cell was pumped down to below $5X10^{-6}$ Torr before each new fill to avoid the possibility of contamination. It was found that there was no noticeable difference in the fluorescence spectrum for a cell that contained a particular gas charge for less than 20 hours and, as a precaution, when extremely low buffer gas pressures were used, the buffer gas charges were changed every 2 hours.

3.3 The Laser System

The laser system consisted of a dye laser pumped by a pulsed N_2 laser. The dye laser, which was built in-house, consisted of an oscillator and a single stage amplifier which were both transversely pumped by the N_2 laser. The oscillator stage was pumped with approximately 10% of the N_2 laser output, with the remainder being used to pump the amplifier. The dye was contained in standard cuvettes (Molectron DL-051) that contained approximately 2.5 cc Stilbene 420, dissolved in methanol at a concentration of $1.8x10^{-3}$ M and supplied by the Exciton Chemical Company. This dye had a maximum lasing intensity at 425nm and a useful wavelength range of 408-453nm. The lifetime of the dye solution was typically 4-6 hours in the amplifier stage and 8-10 hours in the oscillator stage after which the Stilbene solution became degraded and no longer produced an optimal output. The dye solution was stirred using an external rotating magnetic field turning Teflon-coated stirrers in the cuvettes. The dye laser was tuned to the appropriate Rb transition by first using a thermionic diode, and fine-tuning was effected using a piezoelectric element attached to the oscillator grating. The output from the dye laser was passed through an optical fiber into an adjoining room where it was made incident on the vapour-gas mixture in the quartz cell. The 20m long, multi-mode fiber (supplied by the Newport Corporation) was UV-transmitting.

The N_2 laser which acted as the pump for the dye laser, was an in-house built unit which utilized a transverse electrical discharge.

The discharge channel was one meter in length with one end closed by a flat total reflector and the other end (the output window) closed with a flat quartz plate. The laser was operated with a N_2 pressure of approximately 49 Torr and a discharge potential of 15 kV d.c. This produced a 337.1 nm pulsed beam with an approximate cross section of 10mm x 40mm having a maximal power output of 8 mJ in a 8 ns (FWHM) pulse, at a repetition rate of up to 60 Hz. The operation of the N_2 laser was adjusted to provide maximum pumping power for the dye laser.

3.4 The Detection and Data Acquisition System

As may be seen in Fig. (3.1.1), the fluorescence was passed through a piezoelectrically scanned Fabry-Perot interferometer, collimated, filtered with a Schott colour glass filter (BG-18, 1mm thick), and focused onto the photocathode of an ITT FW130 refrigerated photomultiplier. The output of the photomultiplier was amplified by an Ortec 9302 amplifier-discriminator and was sent to an in-house built pulse sampler which accepted an input signal from the photomultiplier P2 and compared this voltage to a set threshold level. The incoming signal was sampled at 5 ns intervals and stored in the static memory of the pulse sampler for that particular interval. After a set number of samples corresponding to the memory size (1024 channels) was accepted, the data were collected in a multichannel scaler. This information was accumulated over the experimental run and then stored in the microcomputer for further analysis of the integrated intensities of the fluorescence components.

The scanning interferometer (Burleigh, model 110) had $\lambda/200$ aluminized mirrors which produced an instrumental finesse of 30. The stability of the interferometer was ensured by having the alignment locked to the interference pattern of a He-Ne laser (Metrologic model ML800) which was scanned at the start of every interferometer sweep and provided the reference for the DAS10 controller. This was accomplished by having the He-Ne reference beam pass through the interferometer before being detected by the second photomultiplier P2 and then having the amplified signal applied to the DAS10 stabilizer as a reference for alignment of the mirrors. The He-Ne laser light was prevented from interfering with the fluorescence detection system by two shutters, S1 positioned in front of the He-Ne laser and S2 placed in front of the photomultiplier P1. The two shutters were controlled by an electronic timer and were locked to the interferometer sweep by the trigger output from the ramp generator. In order to minimize the effects due to the scattered light signals from the dye laser, the pulse inverter amplifier was gated (GATE). This gate was triggered by the photodiode signal produced by the dye-laser output pulses.

The interferometer, which had a free spectral range (FSR) of 17.08 cm^{-1}, was scanned through approximately 3.2 orders of interference. Each scan required approximately 2s during which the photomultiplier output pulses were sent to the MCS whose start was triggered by the interferometer scan and the channel advance rate was synchronized with the triggering of the laser. A few channels at the start of each scan were not used as the DAS10 stabilizer required this time to reset for

each interferometer sweep. Only 512 channels of the possible 1024 on the multichannel scaler were used because of the limitations imposed by the pulse sampler.

It was possible to selectively excite all the individual Zeeman substates and detect their σ-fluorescence components. The background noise of scattered dye-laser light was held at a minimum level by delaying the pulse amplifier signal by 50 ns using a delay box (GATE). This in effect sacrificed the first 20 channels on the MCS, which received no fluorescence signal.

The fluorescence count rate was adjusted to produce a maximum number of counts on the MCS. An average of 20-40 minutes was required to record the fluorescence spectrum resulting from the excitation of a single m_J sublevel and consisting of circularly polarized $\sigma+$ and $\sigma-$ components emitted in the decays of the 6^2P Zeeman states.

3.5 The Superconducting Magnet

The superconducting magnet (an Oxford Instrument NbTi superconducting solenoid, Model S7/123/1) was capable of producing a magnetic field of 7T with a homogeneity of 1% within a 22 mm distance from the centre of the bore which had a 123 mm diameter. The design of the bore allowed the cell and oven assembly to be placed in the magnetic field with direct access to it during the experiment. The entire solenoid was

mounted on a wheeled platform which moved on rails to position the solenoid over the oven assembly which was rigidly attached to the vacuum and gas filling system.

The solenoid was mounted under a 100L liquid-nitrogen (LN) outer container which, along with several heat shields, served as a buffer between the liquid-helium (LH) and the room. The LN boil-off rate was approximately 10.5 L/day and a total of 200 L was required to cool and fill the container. The interior LH vessel held 30L, had a boil-off rate of approximately 3.6 L/day and took approximately 80 L to cool and fill. The LH level had to be closely monitored to ensure that its level never fell below an indicated minimum or a field quench would result, with loss of superconductivity and with the coil receiving the full current load.

Throughout this experiment, the magnetic field strength was held at 4.75T, which required a current of 38 A.

3.6 Use of the Thermionic Diode

The coarse tuning of the dye laser when exciting the Rb $6^2P_{1/2}$ or $6^2P_{3/2}$ fine-structure substate in zero magnetic field was accomplished by observing the fluorescence produced in a hot thermionic diode (TD) (Berends 1988). The TD was used to facilitate the setting of the dye-laser wavelength to the appropriate transitions. The TD operates on the principle of the optogalvanic effect. The pulsed dye-laser light was

focused into the Rb vapour between two electrodes inducing photoionization when an atomic transition was excited. The resulting ions were accelerated by the electric field between the electrodes, gaining sufficient kinetic energy to collisionally ionize other atoms in the cell. This process resulted in an avalanche effect which produced a detectable amplification of the ion current.

Once the wavelength setting was determined with the TD in zero field, the individual Zeeman substates could then be selectively excited in the fluorescence cell in the presence of the magnetic field. The fine tuning to excite a particular Zeeman sublevel was accomplished by maximizing the fluorescence signal while changing the angle of the tuning-grating in the dye-laser oscillator cavity. The optimal setting for a particular Zeeman transition was determined by finding the highest signal count registered from the pulse sampler for different grating angles.

4. Results and Discussion

4.1 Registration of the Zeeman Fluorescence Spectrum

A schematic energy-level diagram of the Rb 6P Zeeman manifold and of the σ-transitions is shown in Fig. (4.1.1). A trace of the fluorescence spectrum resulting from $6^2P_{3/2-3/2}$ excitation and emitted from the Rb atoms in the presence of 120 mTorr Ar is shown in Fig. (4.1.2). The peaks in Fig. (4.1.2) are labelled to correspond to the transitions shown in Fig. (4.1.1). The trace includes 2 interference orders and all six Zeeman components are resolved. A similar trace resulting from $6^2P_{1/2-1/2}$ excitation in the presence of 107 mTorr He is shown in Fig. (4.1.3). Figs (4.1.2) and (4.1.3) show typical Zeeman fluorescence spectra recorded in the course of the experiments and each represents data accumulated during a 45 minute run and consisting of approximately 180,000 counts. The integrated area under each peak was calculated in a computer program using the number of counts accumulated in each channel of the MCS. The resolution of the components in the Zeeman fluorescence spectrum is better than might be apparent from the interferograms in Figs. (4.1.2) and (4.1.3) as the scale has been compressed. The somewhat different intensity patterns in the two spectra suggest that Zeeman mixing within the $^2P_{3/2}$ fs state, which predominates in Fig. (4.1.2), is considerably more efficient than the mixing within the $^2P_{1/2}$ state or between the fs states. Approximately 35 spectra similar to those shown in Figs (4.1.1) and (4.1.2) were recorded, arising from Zeeman mixing induced by He, Ne and Ar collisions.

Fig. (4.1.4) shows a composite Zeeman fluorescence spectrum obtained with all six possible σ excitations in the presence of Ne. The exciting transitions are indicated in the figure and correspond to those shown in Fig. (4.1.1). The fluorescence spectrum resulting from $6^2P_{+1/2}$ excitation (a) was recorded at a buffer gas pressure of 172 mTorr while the spectrum resulting from $6^2P_{+3/2}$ excitation (b) was recorded at a buffer gas pressure of 44 mTorr. It may be seen that $^2P_{1/2}$ Zeeman mixing is difficult to observe at low buffer gas pressures at which I was not able to measure the integrated intensities of the components. The buffer gas pressures at which the integrated intensities could be determined varied, but for the $6^2P_{1/2}$ states I had to use pressures higher than 80 mTorr, while for the $6^2P_{3/2}$ states I used pressures in the range 40 mTorr $< p <$ 260 mTorr. Accordingly, the $6^2P_{1/2}$ Zeeman spectra could not be properly recorded and analyzed at low buffer gas pressures at which the data were either not available or were burdened with a large experimental error.

Fig 4.1.1 Schematic diagram of the energy levels of the 6^2P Zeeman substates in rubidium, showing σ transitions between the 5^2S and 6^2P Zeeman substates. Only the $6^2P_{1/2,-1/2}$ (B) and $6^2P_{3/2,-3/2}$ (E) excitations are indicated; the π transitions are not shown and the spacing between the levels is not drawn to scale.

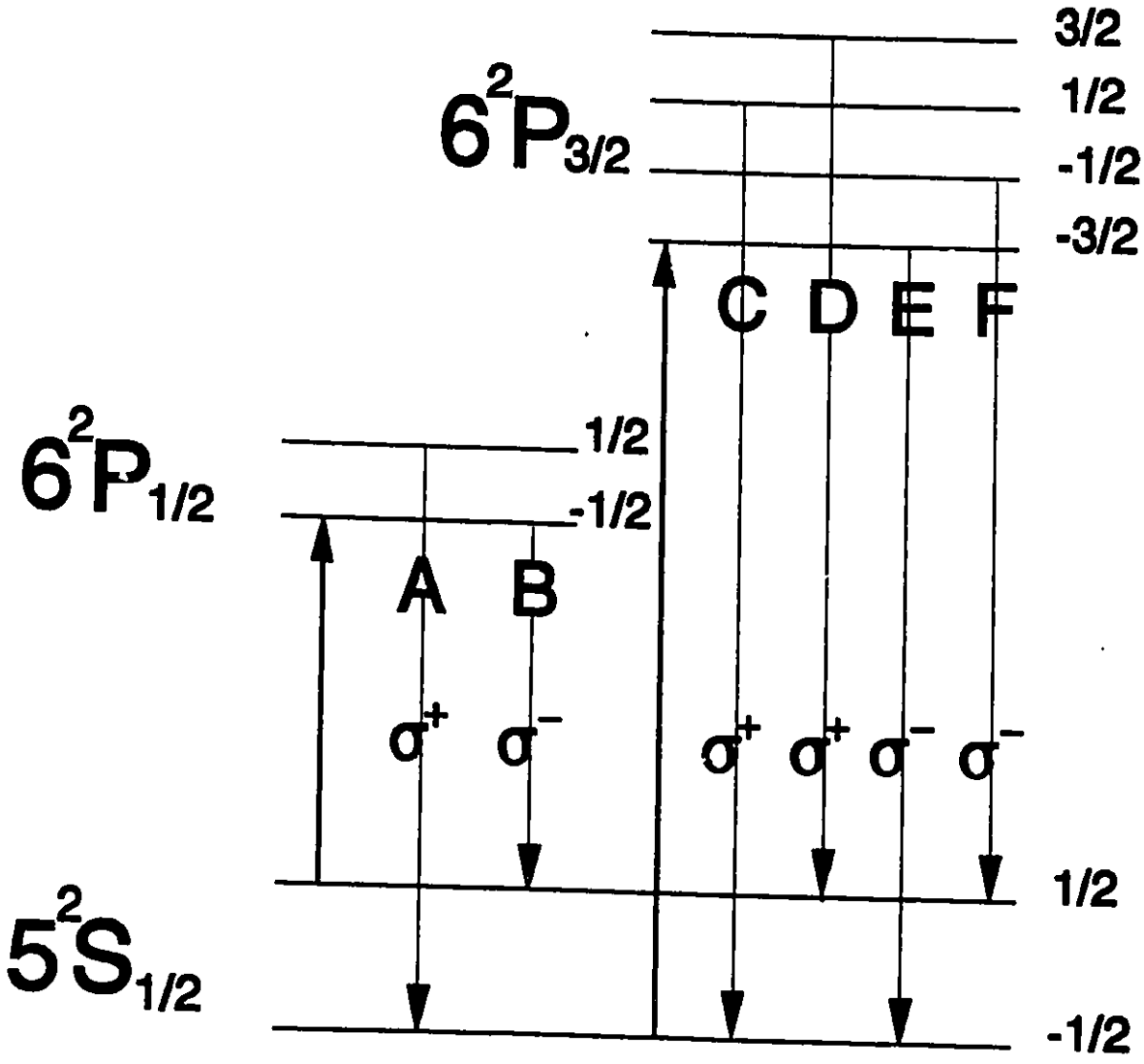
$6^2P_{3/2}$
3/2
1/2
-1/2
-3/2
C D E F
$6^2P_{1/2}$
1/2
-1/2
A B
σ^+ σ^-
σ^+ σ^+ σ^- σ^-
$5^2S_{1/2}$
1/2
-1/2

Fig 4.1.2 A trace of the Zeeman fluorescence spectrum emitted from rubidium vapour mixed with 120 mTorr Ar. The $6^2P_{3/2,-3/2}$ state was optically excited and the peaks are labelled to correspond to the transitions indicated in Fig (4.1.1). The peaks labelled E are due to the decay of the primarily excited $6^2P_{3/2,-3/2}$ Zeeman state, the other peaks are due to collisional Zeeman mixing. The free spectral range (FSR) of the interferometer was 17.08 cm^{-1}.

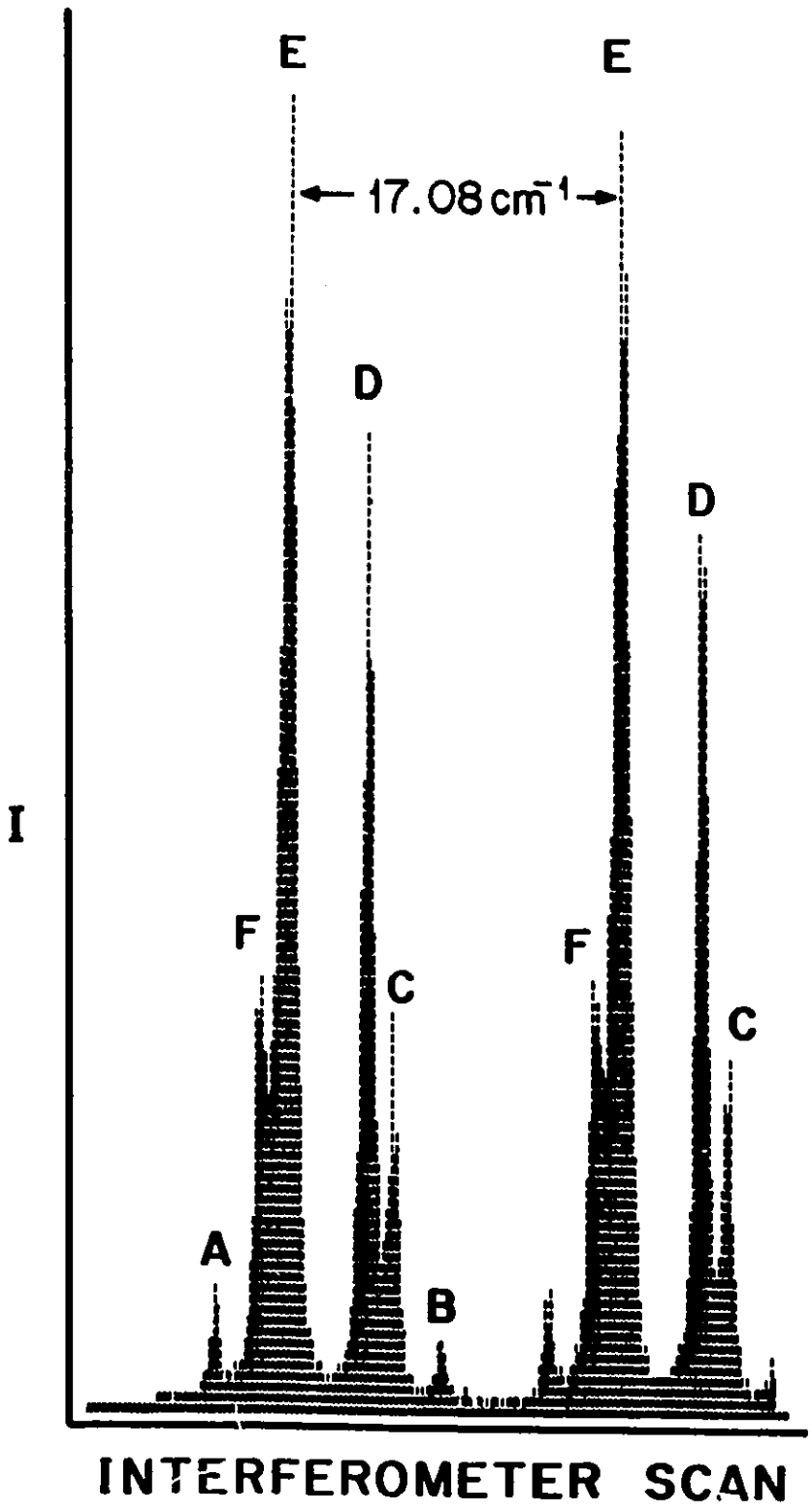
E
E
17.08 cm⁻¹
D
D
I
F
F
C
C
A
B
INTERFEROMETER SCAN

Fig 4.1.3 A trace of the Zeeman fluorescence spectrum emitted from rubidium vapour mixed with 107 mTorr He. The $6^2P_{1/2,-1/2}$ state was optically excited and the peaks are labelled to correspond to the transitions indicted in Fig (4.1.1). The peaks labelled B are due to the decay of the primarily excited $6^2P_{1/2,-1/2}$ Zeeman state, the other peaks are due to collisional Zeeman mixing.

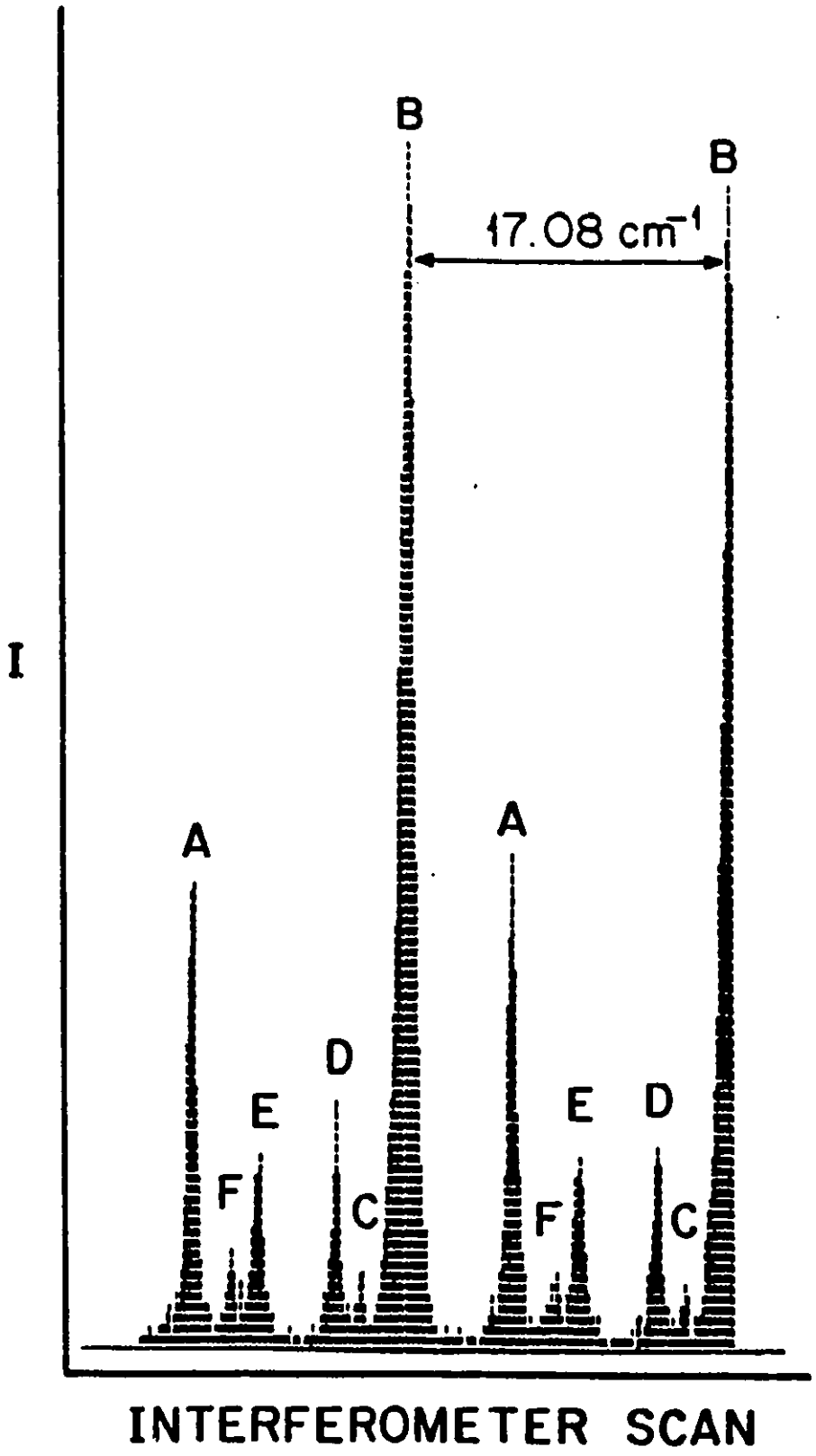
B
B
17.08 cm⁻¹
I
A
A
D
E
F
C
E
D
F
C
INTERFEROMETER SCAN

Fig 4.1.4 A composite Zeeman fluorescence spectrum. (a), $6^2P_{1/2}$ excitation, 172 mTorr Ne. (b), $6^2P_{3/2}$ excitation, 44 mTorr Ne. The Components A-F correspond to the σ transitions identified in Fig. 4.1.1. Each component was separately excited and the resulting fluorescence spectra (one interference order for each) were combined to produce the composite.

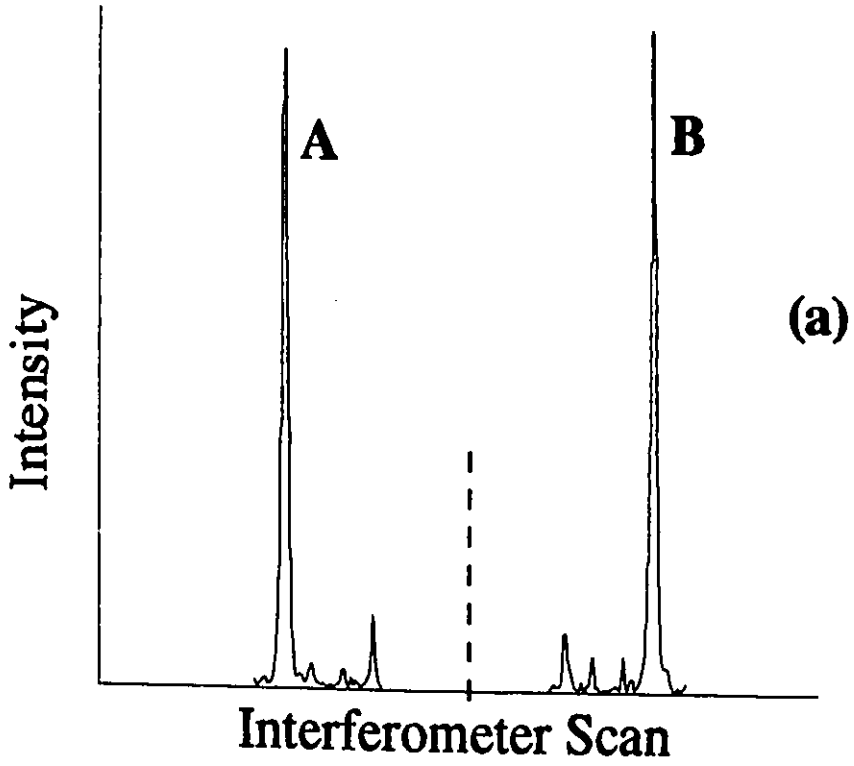
A
B
Intensity
(a)
Interferometer Scan

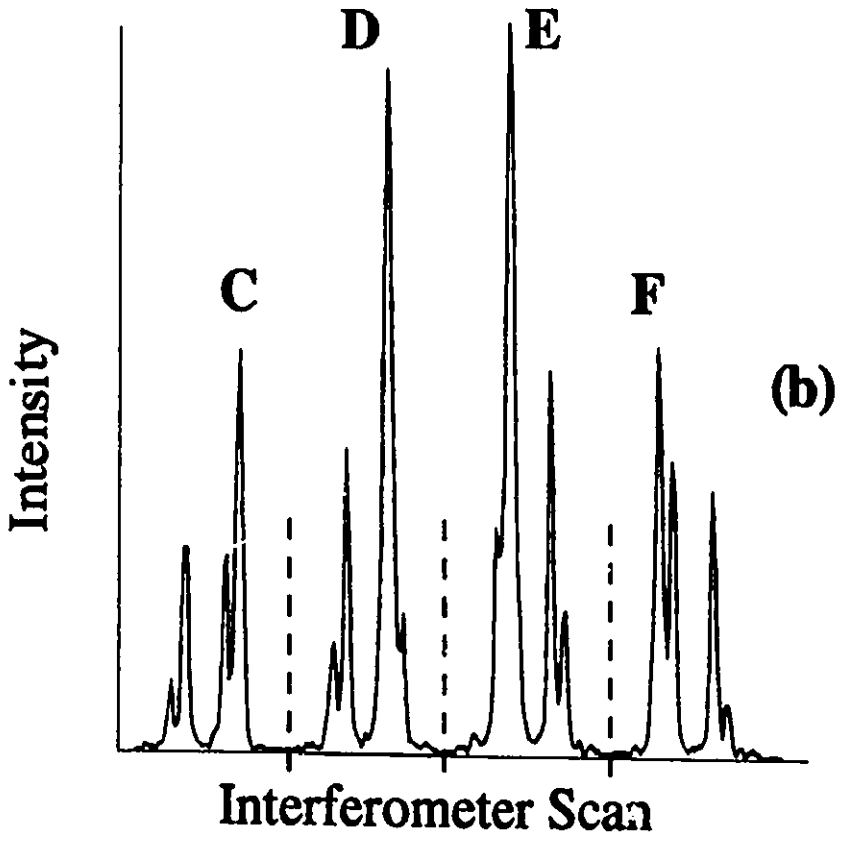
D
E
C
F
Intensity
(b)
Interferometer Scan

4.2 Data Reduction and Calculations

The integrated intensities of all the components of the fluorescence spectra were normalized to ensure consistent results from differing intervals of time used for their recording. Normalizing the raw experimental data involved taking the number of photon counts detected in each integrated intensity interval and dividing by the number of sweeps of the multichannel scaler. This makes possible an easy comparison of the spectral intensities for differing buffer gas pressures as each peak now represents a number of photons detected per sweep of the MCS. The normalized integrated intensity ratios of sensitized-to-direct fluorescence components in the spectra were then multiplied by the appropriate ratios of the Einstein $A^{s}_{J,m}$ coefficients and are plotted against buffer-gas pressures in Figs. (4.2.1 - 4.2.3). These figures represent typical plots of population ratios of collisionally-to-directly (optically) populated Zeeman sublevels in the 6^2P Zeeman manifold. The linearity of the data in the plots suggests the absence of multiple-collisional excitation transfers, including back transfer. The various individual Zeeman mixing cross sections $Q(J,m \rightarrow J',m')$ were calculated by substituting the data into eq.(2.2.6) and subjecting them to a weighted linear regression fit over the range of buffer gas pressures where the population ratios remained linear with $N\upsilon\tau$. It was found that, over moderate buffer gas pressures, the slopes of plots of population ratios against $N\upsilon\tau$ were linear within experimental error. At pressures higher than those shown in Figs. (4.2.1 - 4.2.3), the sublevels became saturated and the plots assumed a downward curvature,

tending to a slope of zero. Data obtained at such higher pressures, at which single collision conditions were not maintained, were not used in the calculations of the Zeeman mixing cross sections.

The Zeeman mixing cross sections are listed in Tables (4.2.1) and (4.2.2) and it may be seen that, in all cases, the cross sections are the largest for He and the smallest for Ne, a trend which has also been observed in other experiments (Berends et al. 1988; Skalinski and Krause 1982). Some of the Zeeman mixing cross sections are burdened by large uncertainties, which are due to overlap of some of the spectral components, as may be seen in Fig. (4.1.4), particularly among the $6^2P_{3/2}$ peaks. To reduce the effects of this overlap, the intensities were integrated over only 5 channels of the MCS, which reduced the contributions from adjacent fluorescence peaks. In cases where the peaks actually overlapped, as was the case with many F peaks, the overlapping components were separated by subtraction.

It is clear from Tables (4.2.1) and (4.2.2) that cross sections for mixing between the m_J levels of the $^2P_{1/2}$ and $^2P_{3/2}$ fs states are smaller than the cross sections for mixing within the $^2P_{1/2}$ state, and the cross sections for mixing within the $^2P_{3/2}$ state are the largest of all. This was to be expected since the 6^2P fs splitting (77 cm^{-1}) is relatively large; while it is smaller than kT at the temperature of the fluorescing vapour-gas mixture (269 cm^{-1}), it is non-negligible compared to the inverse collision time. That the cross sections for m_J mixing within the $^2P_{1/2}$ state are significantly smaller than within the

$^2P_{3/2}$ state may be due to the $m_j \leftrightarrow -m_j$ transitions being forbidden, as has been indicated in some earlier theoretical studies (Franz and Franz 1966; Franz et al. 1967; Elbel and Naumann 1967). On the other hand it has been suggested that these transitions are made possible by magnetic-field-induced $^2P_{1/2}$ - $^2P_{3/2}$ virtual mixing, a process which has been found to be magnetic-field dependent (Guiry and Krause 1975).

The multipole relaxation cross sections may be calculated from the m_j mixing cross sections listed in Tables (4.2.1) and (4.2.2). This was done using eqs. (2.2.8) through (2.2.11) and the resulting multipole relaxation cross sections are presented in Table (4.2.3). Theoretical calculations indicate that, for $P_{3/2}$ relaxation, the quadrupole relaxation component should be the largest (Baylis 1979). In other experimental low-field work (B=0.11T), Kamke (1975) found that the quadrupole relaxation component was consistently larger than the dipole component, but no values for the octupole component were given. This trend, noted in Na(3P) collisions with noble gas (Gay and Schneider 1976), and in K(4P) collisions by Skalinski and Krause (1982) and Boggy and Franz (1982), is not so clearly borne out in the present experiment. Here, the quadrupole relaxation cross sections are largest for the He collisions, but the cross sections for the octupole relaxation are largest for both Ne and Ar, as was previously reported by Berends et al. (1989), though the large uncertainty in the multipole relaxation cross sections may mask their true trend. Tables (4.2.1) and (4.2.2) also show the

theoretical cross section calculations of Pascale (1987). Although the theoretical cross sections are in each case smaller than the experimental ones, they do follow the same general trend.

The multipole relaxation cross sections listed in Table (4.2.3) show different behaviour from those for collisions of K(5P) of Berends et al. (1989). Generally, the monopole component is smaller than in the K(5P) experiment while the dipole, quadrupole and octupole components are roughly three times larger. Also shown in Table (4.2.3) are the multipole relaxation cross sections calculated from eqs. (2.2.13 - 2.2.16). These cross sections all lie within the uncertainty of the other calculated cross sections from eqs. (2.2.8 - 2.2.11). The error limits accompanying these experimentally determined cross sections were derived from the weighted sums of the standard deviations for the individual Zeeman mixing cross sections.

The fs transfer cross sections, $\sigma^{(0)}$ were derived from the Zeeman mixing cross sections using eqs. (2.2.22 - 2.2.25) and are listed in Table (4.2.4). Also listed are the experimental values of Siara (1972), which were determined in zero field and which are smaller. A similar discrepancy between zero-field and high field values has been noted previously in similar work with potassium (Berends 1988) and this leads to speculation whether the fs mixing process might not be affected by the strong magnetic field (Siara, Hrycyshyn and Krause 1972).

Fig 4.2.1 Plots of Zeeman fluorescence intensity (and population) ratios, arising from $6^2P_{3/2,+3/2}$ excitation, showing effects of Zeeman mixing by Rb-Ar collisions. The separate origin for each plot is indicated on the vertical axis. The error bars represent statistical scatter of the measurements. Each point represents the intensity ratio of the specified components, multiplied by the ratio of the appropriate $A^{s}_{J,m}$ coefficients. (a), I(A)/I(D); (b), I(B)/I(D); (c), I(E)/I(D); (d), I(C)/I(D); (e), I(F)/I(D).

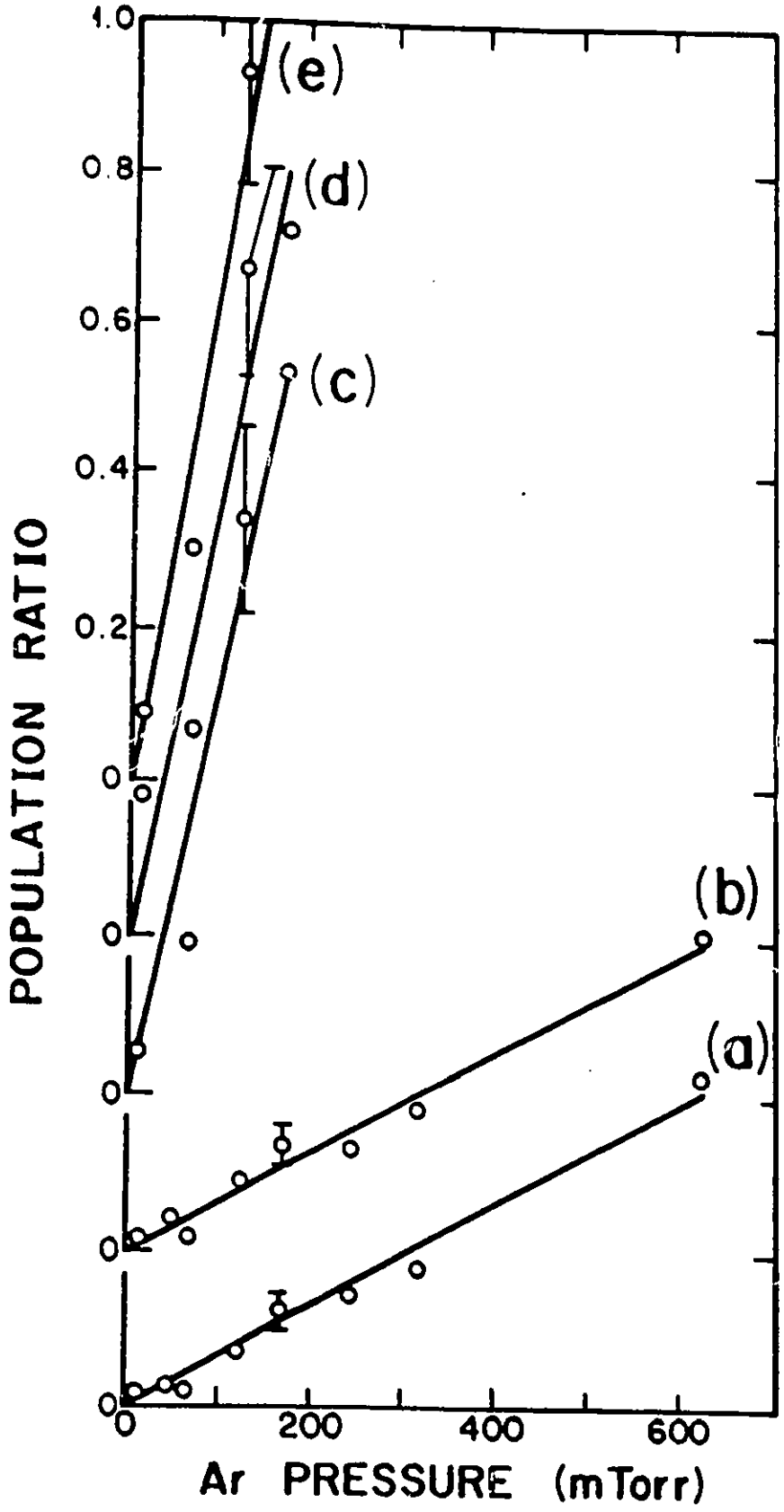
1.0
0.8
0.6
0.4
0.2
0
0
0
0
0
(e)
(d)
(c)
(b)
(a)
POPULATION RATIO
0
200
400
600
Ar PRESSURE (mTorr)

Fig 4.2.2 Plots of Zeeman fluorescence (and population) ratios, arising from $6^2P_{3/2,+1/2}$ excitation, against Ne pressure. For a description see Fig (4.2.1). (a), I(B)/I(C); (b), I(A)/I(C); (c), I(D)/I(C); (d), I(E)/I(C); (e), I(F)/I(C).

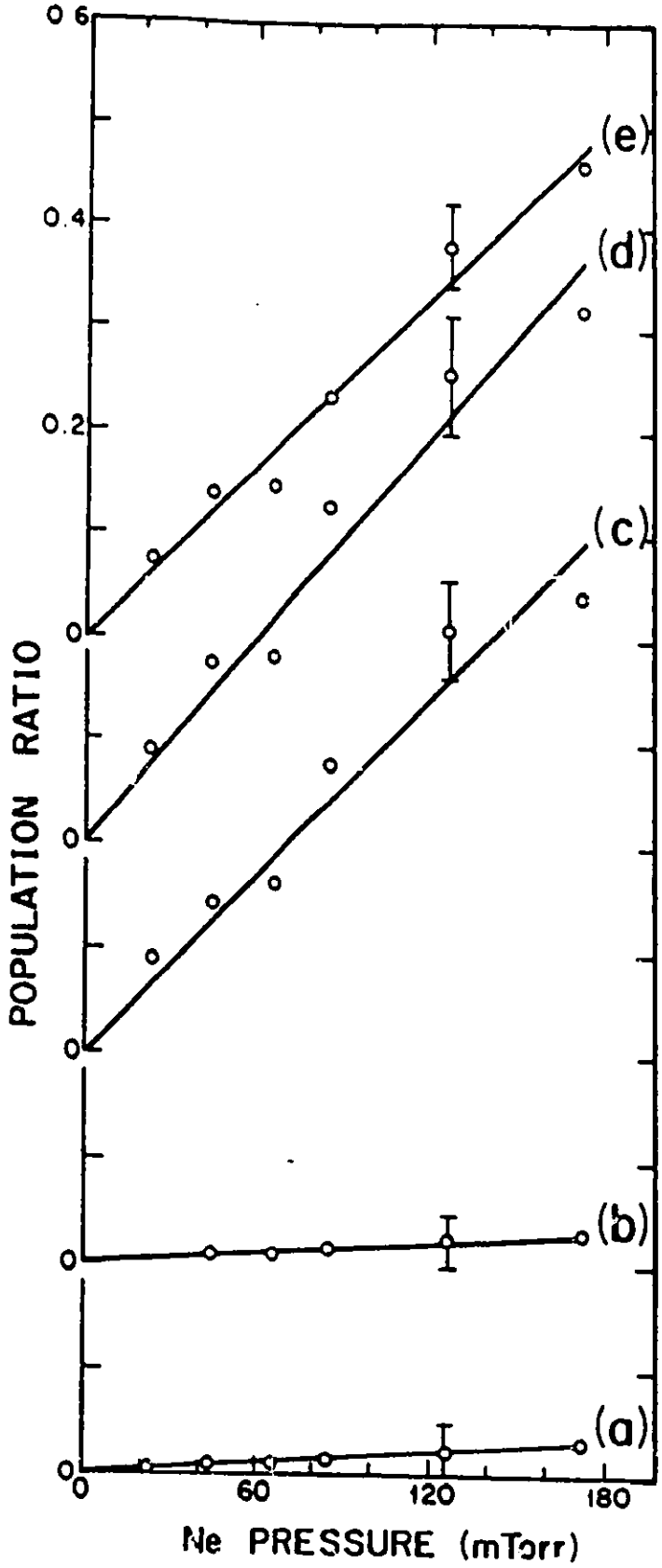
0.6
0.4
0.2
0
0
0
0
0
(e)
(d)
(c)
(b)
(a)
POPULATION RATIO
0
60
120
180
Ne PRESSURE (mTorr)

Fig 4.2.3 Plots of Zeeman fluorescence (and population) ratios, arising from $6^2P_{3/2,+1/2}$ excitation, against He pressure. For a description see Fig (4.2.1). (a), I(A)/I(C); (b), I(B)/I(C); (c), I(D)/I(C); (d), I(E)/I(C); (e), I(F)/I(C).

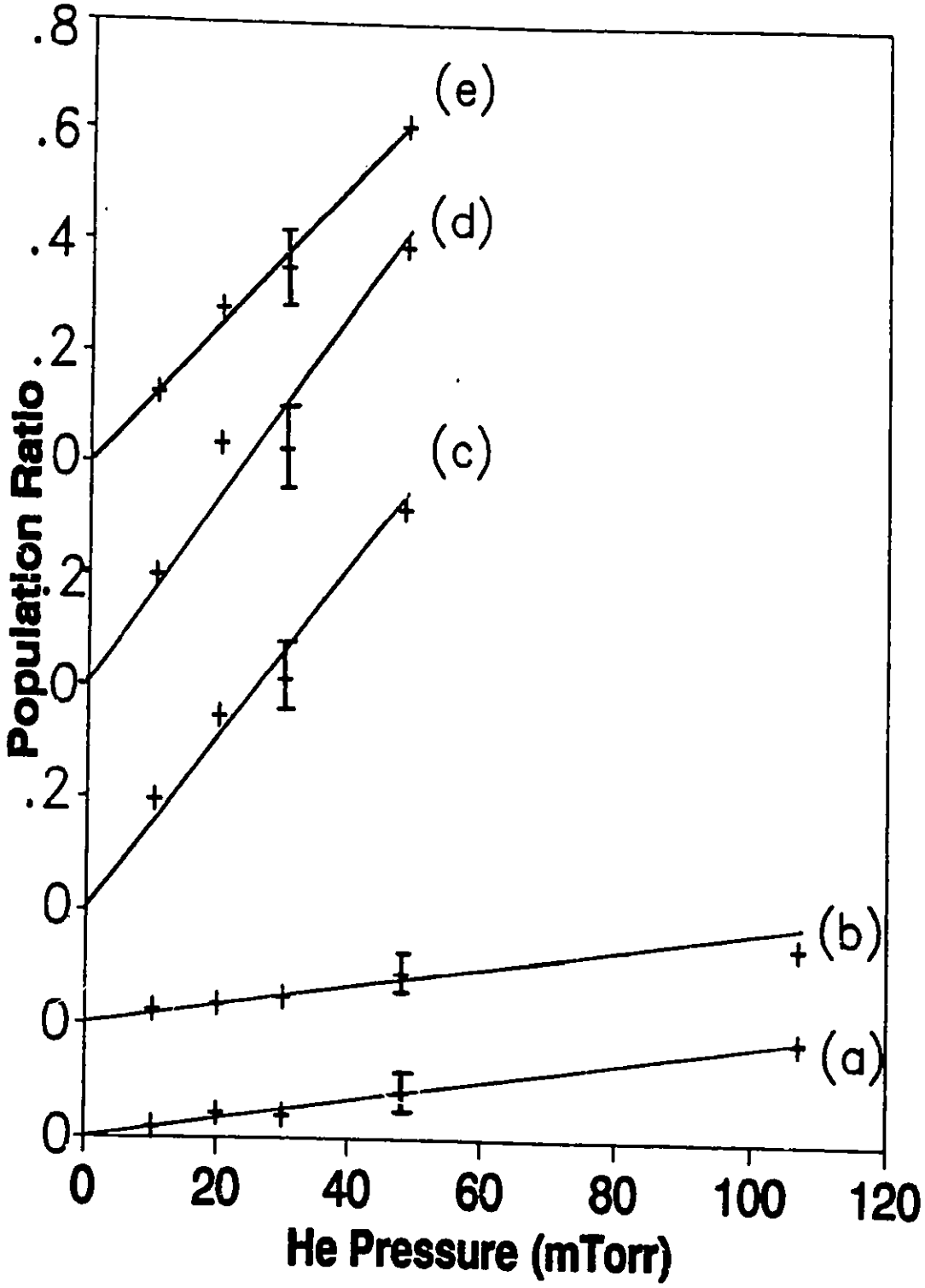
.8
.6
.4
.2
0
.2
0
.2
0
0
(e)
(d)
(c)
(b)
(a)
Population Ratio
0
20
40
60
80
100
120
He Pressure (mTorr)

TABLE 4.2.1 6P Zeeman Mixing Cross Sections for Collisions with He, Ne and Ar. ($10^{-16}\,cm^2$)

$Q(J,m \rightarrow J',m')$ *for* $J = 1/2,\ m = \pm 1/2$

Designation $Q(J,m \rightarrow J',m')$	Collision Partner		
	He	Ne	Ar
$Q(1/2+1/2 \rightarrow 1/2-1/2)$	129 ± 40	27 ± 8	34 ± 10
$Q(1/2+1/2 \rightarrow 3/2+1/2)$	46 ± 15	7 ± 2	14 ± 4
$Q(1/2+1/2 \rightarrow 3/2+3/2)$	51 ± 20	6 ± 1	14 ± 3
$Q(1/2+1/2 \rightarrow 3/2-3/2)$	58 ± 20	8 ± 1.5	22 ± 6
$Q(1/2+1/2 \rightarrow 3/2-1/2)$	51 ± 10	*	21 ± 5
$Q(1/2-1/2 \rightarrow 1/2+1/2)$	83 ± 40; 49.4[a]	28 ± 8	35 ± 10
$Q(1/2-1/2 \rightarrow 3/2+1/2)$	20 ± 6; 6.8[a]	9 ± 2.5	20 ± 5
$Q(1/2-1/2 \rightarrow 3/2+3/2)$	23 ± 5; 7.9[a]	7 ± 1.5	16 ± 3
$Q(1/2-1/2 \rightarrow 3/2-3/2)$	25 ± 5; 4.7[a]	7 ± 2	17 ± 3
$Q(1/2-1/2 \rightarrow 3/2-1/2)$	25 ± 5; 5.8[a]	7 ± 1.5	17 ± 5

*-relevant fluorescent line was obscured.

Ref.: [a]Pascale (1987).

TABLE 4.2.2 6P Zeeman Mixing Cross Sections for Collisions with He, Ne and Ar. ($10^{-16}\,cm^2$)

$Q(J,m \rightarrow J',m')$ *for* $J = 3/2$, $m = \pm 1/2, \pm 3/2$

Designation $Q(J,m \rightarrow J',m')$	Collision Partner		
	He	Ne	Ar
Q(3/2+1/2→1/2+1/2)	50 ± 13	9 ± 2.5	16 ± 5
Q(3/2+1/2→1/2−1/2)	45 ± 13	9 ± 3	16 ± 5
Q(3/2+1/2→3/2+3/2)	438 ± 85	140 ± 30	218 ± 45
Q(3/2+1/2→3/2−3/2)	521 ± 100	163 ± 30	155 ± 30
Q(3/2+1/2→3/2−1/2)	334 ± 65	136 ± 30	140 ± 30
Q(3/2+3/2→1/2+1/2)	76 ± 24	16 ± 5	32 ± 9
Q(3/2+3/2→1/2−1/2)	*	17 ± 5	32 ± 9
Q(3/2+3/2→3/2+1/2)	*	*	292 ± 115
Q(3/2+3/2→3/2−3/2)	*	244 ± 50	272 ± 100
Q(3/2+3/2→3/2−1/2)	*	296 ± 60	343 ± 120
Q(3/2−3/2→1/2+1/2)	42 ± 20; 10.4[a]	*	34 ± 15
Q(3/2−3/2→1/2−1/2)	31 ± 9; 5.2[a]	*	22 ± 7
Q(3/2−3/2→3/2+1/2)	378 ± 75; 147.1[a]	187 ± 35	285 ± 50
Q(3/2−3/2→3/2+3/2)	283 ± 55; 71.5[a]	185 ± 35	212 ± 105
Q(3/2−3/2→3/2−1/2)	425 ± 210; 165[a]	311 ± 90	374 ± 180
Q(3/2−1/2→1/2+1/2)	49 ± 10; 9.1[a]	9 ± 2.5	12 ± 3.5
Q(3/2−1/2→1/2−1/2)	39 ± 10; 7.6[a]	8 ± 2.5	11 ± 3
Q(3/2−1/2→3/2+1/2)	287 ± 80; 94.9[a]	129 ± 25	115 ± 30
Q(3/2−1/2→3/2+3/2)	341 ± 100; 147.1[a]	159 ± 30	*
Q(3/2−1/2→3/2−3/2)	492 ± 50; 165[a]	174 ± 35	*

*-relevant fluorescent line was obscured.

Ref.: [a]Pascale (1987).

TABLE 4.2.3 6^2P Multipole Relaxation Cross Sections (10^{-16} cm^2)

Designation	Ref.	Collision Partner		
		He	Ne	Ar
$\Lambda^{(1)}_{1/2}$	a	166 ± 80	56 ± 16	70 ± 20
	b	258	54	68
$\Lambda^{(1)}_{3/2}$	a	1353 ± 350	827 ± 177	1053 ± 397
	b	1342	782	977
$\Lambda^{(2)}_{3/2}$	a	1606 ± 570	996 ± 250	1318 ± 460
	b	*	*	1154
$\Lambda^{(3)}_{3/2}$	a	1510 ± 1100	1240 ± 500	1350 ± 1030
	b	1404	842	831

*-relevant fluorescent line was obscured.
Ref.: a-this experiment, eqs. (2.2.8-11).
b-this experiment, eqs. (2.2.13-16).

TABLE 4.2.4 6P Fine Structure Mixing Cross Sections ($10^{-16} cm^2$)

Designation	Ref.	Collision Partner		
		He	Ne	Ar
$\sigma_{21}^{(0)}\left(\frac{3}{2}\rightarrow\frac{1}{2}\right)$	a	66 ± 15	21 ± 5	49 ± 11
	b	19.0	6.4	14.9
$\sigma_{12}^{(0)}\left(\frac{1}{2}\rightarrow\frac{3}{2}\right)$	a	103 ± 41	*	79 ± 17
	b	29.3	10.3	24.0

*-relevant fluorescent line was obscured.
Ref.: a-this experiment, eqs (2.2.22-23)
b-Siara (1972).

4.3 Sources of Experimental Error

The uncertainty attributed to the cross sections listed in Tables (4.2.1-4) arises from both statistical and systematic errors. The systematic errors include the experimentally determined constants used in the calculations such as the lifetimes of the various states. The statistical errors can be attributed to stray (scattered) light, and fluctuations in laser intensity and oven temperature. The systematic errors were due mostly to the uncertainty in the lifetimes of the states (~6%), in the measured pressures (~4%) and in the measured oven temperature (~1%). These uncertainties combine to give an error in the calculated Zeeman mixing cross sections in Table (4.2.1-2) estimated to be of the order of up to 30% most of which is due to statistical error.

There were several sources of statistical error. The laser power fluctuations in the N_2 pump laser can account for a small part of this error which was kept at a minimum since the pump laser was not allowed to cool down in between the experimental runs and the laser-dye was changed when count rates dropped during a run. The major source of uncertainty in the Zeeman mixing cross sections arose from the determinations of the scattered radiation intensity. The excitation of any of the σ substates within the 6P Zeeman manifold resulted in some scattered radiation. This scattered radiation ranged in value from just a few percent to over 30% over all the Zeeman mixing cross sections and for all buffer gases. These percentages were determined by directly exciting the π transitions in the 6P manifold. For each buffer gas

and at each pressure used to record the spectra, the dye laser was tuned to also excite the various π transitions which are shown in Fig. (4.3.1).

The ability to excite all the σ and all the π transitions made possible the determination of the intensity of the scattered radiation which was always present in this experiment. The direct excitation of selective σ transitions followed by the detection of σ-fluorescence caused some difficulties since, with zero time-delay between excitation and detection, the detector was saturated with scattered laser radiation which swamped the fluorescence. When a π transition is directly excited ($\Delta m_J = 0$) then the scattered laser radiation is of different wavelength than all the σ-fluorescence components, making possible a more precise determination of fluorescence intensities. In this experiment I used a time-delay between the excitation and the detection of the fluorescence to limit the amount of scattered laser light. This procedure has been used previously (Berends 1988) with the result that most of the scattered stray laser light was eliminated. Fig. (4.3.2) shows two Zeeman fluorescence spectra: one obtained with π excitation and the other with σ excitation. It may be seen that with π excitation, the peak corresponding to the scattered laser light is displaced from the σ fluorescence peaks while with σ-excitation the scattered light is overlaid on the direct fluorescence component. The fluorescence interferograms obtained with π excitation were used as overlays for the σ excitation spectra in order to estimate the relative

intensity of the fluorescence signal compared with the scattered laser radiation. Using this method I found that the stray light varied from 8% to 30% of the fluorescence intensity.

Fig 4.3.1 Schematic diagram of the Zeeman splitting of the 5^2S and 6^2P states in rubidium, showing the σ and π transitions. The energy separations are not drawn to scale.

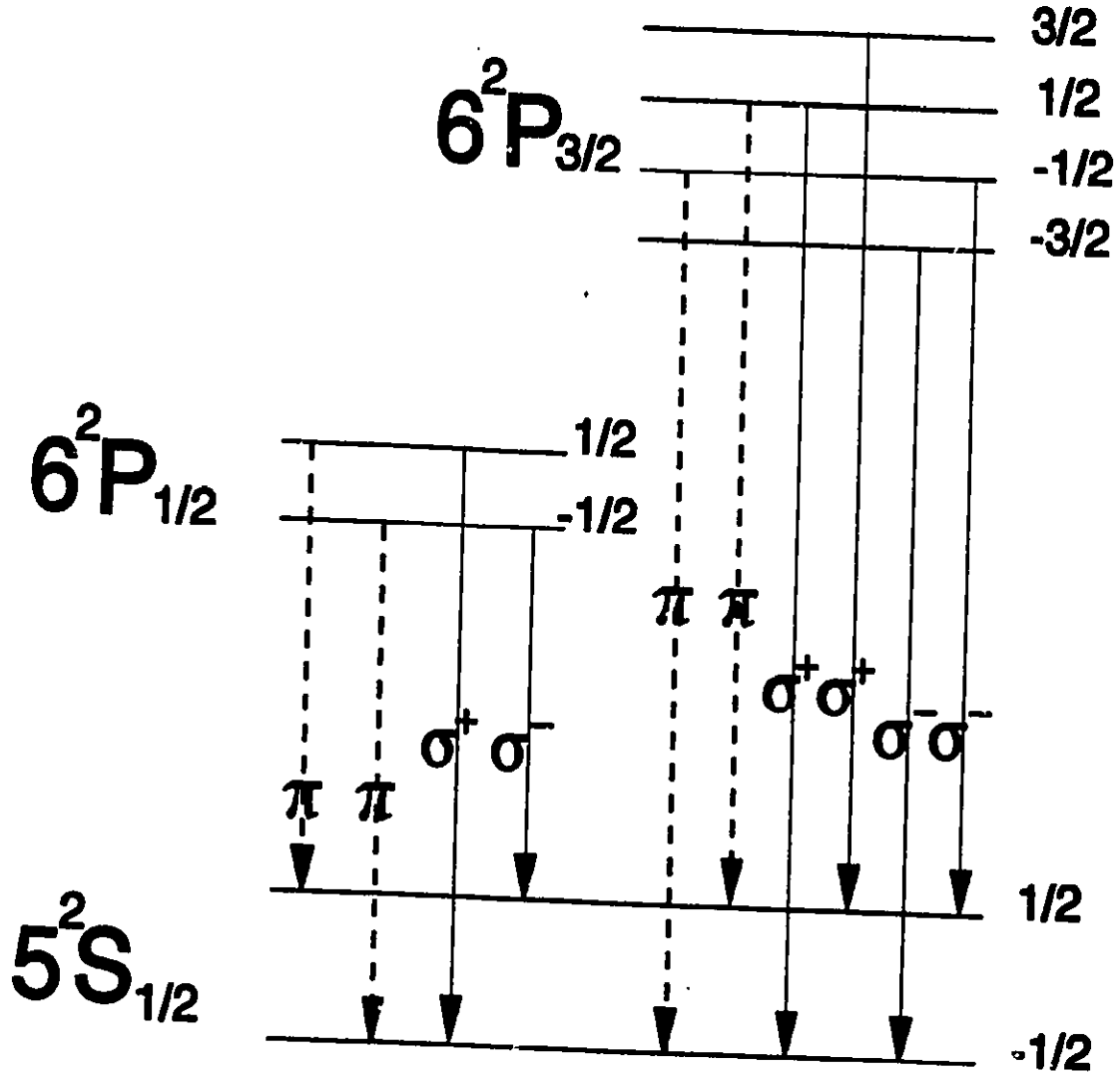
3/2
1/2
-1/2
-3/2
$6^2P_{3/2}$
$6^2P_{1/2}$
1/2
-1/2
π
π
σ^+
σ^-
π
π
σ^+
σ^+
σ^-
σ^-
$5^2S_{1/2}$
1/2
-1/2

Fig 4.3.2 Traces of the Zeeman fluorescence spectrum emitted from rubidium vapour mixed with 172 mTorr Ne. (a), σ-exciation; (b), π-excitation

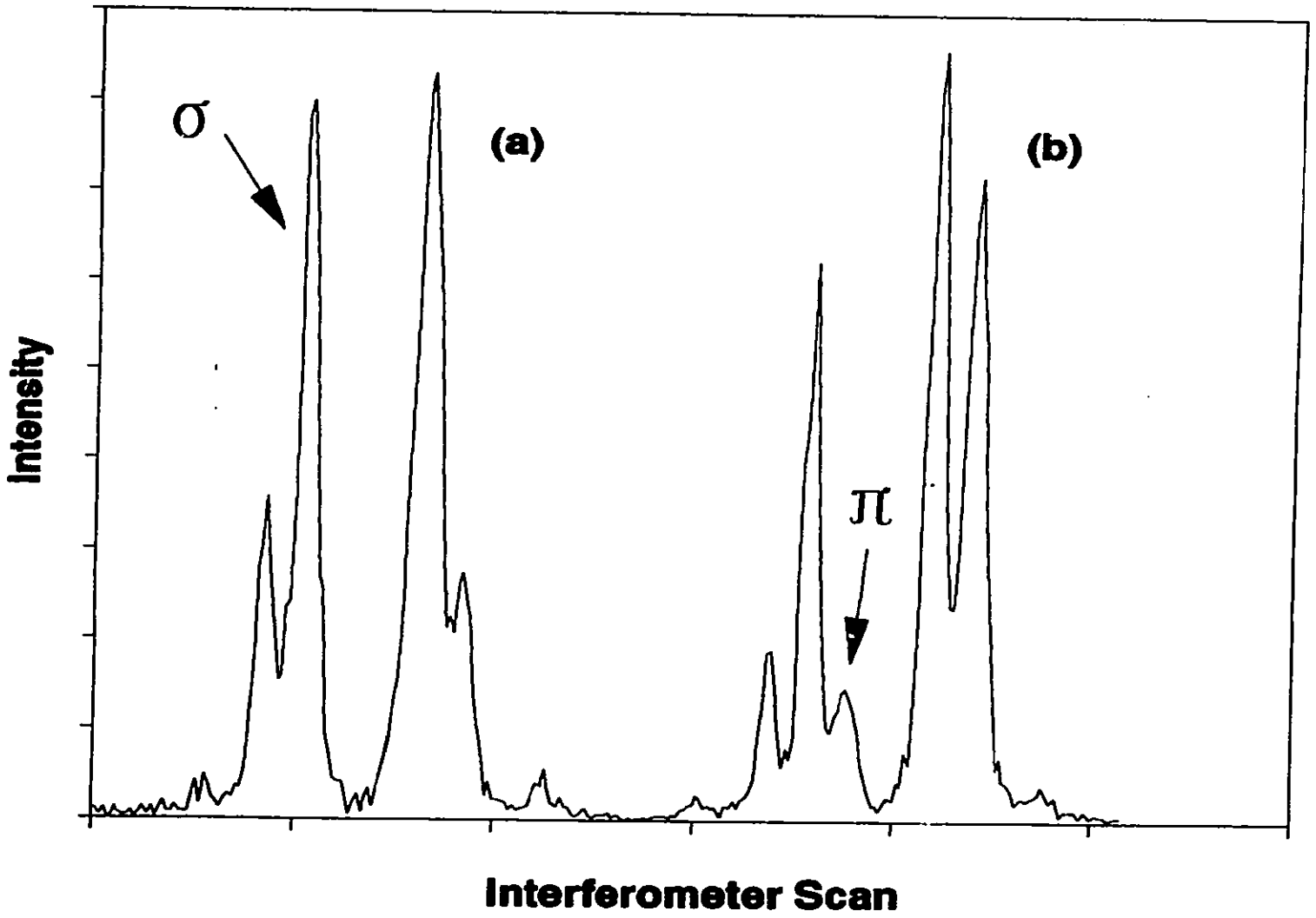
σ
(a)
(b)
π
Intensity
Interferometer Scan

5. Conclusions

This thesis describes an experiment in which the collisional relaxation of the atomic multipole moments associated with the 6P states of rubidium were investigated in a magnetic field of 4.75 T. The experimental data yielded the cross sections for the fs mixing, Zeeman mixing, and multipole relaxation of 6P rubidium atoms, by collisions with noble gas atoms.

All cross section measurements were carried out in a laser-spectroscopic experiment. This entailed utilizing a photon-counting technique which employed a pulsed dye laser and a scanning Fabry-Perot interferometer. Determination of the relative intensities of the spectral components in the Zeeman fluorescence spectrum allowed the calculation of cross sections for Zeeman mixing and for collisional multipole relaxation. The various cross sections determined in this experiment are summarized in Tables (4.2.1 - 4.2.4). The cross sections are subject to considerable experimental error arising from scattered laser light and from the overlap between components of the spectra.

This study is believed to be the first direct experimental determination of the Zeeman mixing cross sections and multipole-relaxation cross sections for the 6^2P states in Rb atoms colliding with noble-gas atoms.

Bibliography

Banwell C. N., 1983, Fundamentals of Molecular Spectroscopy, 3rd ed., McGraw-Hill, London

Baylis W. E., 1978, "Interatomic Potentials for Collisions of Excited Atoms", in Progress in Atomic Spectroscopy Part. A, Eds, W. Hanle and H. Kleinpoppen, Plenum Press, New York

Baylis W. E., 1979, "Collisional Depolarization in the Excited State", in Progress in Atomic Spectroscopy Part. B, Eds, W. Hanle and H. Kleinpoppen, Plenum Press, New York

Berdowski W., Shiner T. and Krause L., 1971, Phys. Rev. A 4, 984

Berends R.W., 1988, Ph.D. Thesis, University of Windsor, Ontario

Berends R.W., Kedzierski W. and Krause L., 1988, Phys. Rev. A 37, 68

Berends R.W., Kedzierski W., Baylis W.E., and Krause L., 1989, Phys. Rev. A 39, 1526

Boggy R. and Franz F.A., 1982, Phys. Rev. A 25, 1887

Bucka H., Grossivendt B., and Schuessler H.A., 1966, Z. Physik, 194, 193

Bulos R. B. and Happer W., 1971, Phys. Rev. A 4 849

Elbel M., 1979, "Energy and Polarization Transfer" in Progress in Atomic Spectroscopy Pt. B, Eds W. Hanle and H. Kleinpoppen, Plenum Press, New York

Elbel M. and Naumann F., 1967, Z. Phys. 204, 501

Franz F.A. and Franz J.R., 1966, Phys. Rev. 148, 82

Franz F.A., Leutert G., and Shuey R., 1967, Helv. Phys. Acta 40, 779

Gallagher J.H., 1969, Ph.D. Thesis, University of Colorado, Colorado

Gay J.C. and Schneider W.B. 1976, Z. Phys. A. 278, 211

Guiry J. and Krause L., 1972, Phys. Rev. A 6, 273

Guiry J. and Krause L., 1975, Phys. Rev. A 12, 2407

Jordan, Jr. J.A., 1964, Ph.D. Thesis, University of Michigan, Michigan

Kamke B. Z., 1975, Physik 273, 23

Krause L., 1975, in The Excited State in Chemical Physics, Ed. J. Wm. McGowan, John Wiley and Sons, Inc., Chapter 4.

Lochte-Holtgreven W.Z., 1928, Physik 47, 362

Mitchell A.C.G. and Zemansky M.W., 1934, Resonance Radiation and Excited Atoms, Cambridge University Press, Cambridge

Migdalek J. and Baylis W. E., 1979, Can. J. Phys. 57, 1708

Pascale J. and Vandeplanque J., 1974, J. Chem. Phys. 60, 2278

Pascale J., 1987, Private communication

Rebentrost F., Best R. and Happer W., 1987, J. Phys. B: At. Mol. Phys. 20, 2627

Seiwert R., 1956, Ann. Physik 18, 54

Siara I., 1972, Ph.D. Thesis, University of Windsor, Ontario

Siara I., Hrycyshyn E.S. and Krause L., 1972, Can. J. Phys. 50, 1826

Skalinski P. and Krause L., 1982, Phys. Rev. A 26, 3338

Spielfiedel A., Gilbert D., Roueff E. and F. Rostas, 1979, J. Phys. B: At. Mol. Phys. 12, 3693

Thangaraj M.A., 1948, Ph.D. Thesis, University of Toronto, Ontario

Wood R.W., 1922, Phil. Mag. 44, 1107

Wood W. and Mohler F.L., 1918, Phys. Rev. 11, 70

Woodgate G.K., 1980, Elementary Atomic Structure, 2nd Ed., Clarendon Press, Oxford

APPENDIX A

Zeeman Splitting of the 6P States

The magnetic dipole moment of an atom can be represented by a vector $\vec{\mu}$ which is directly proportional to the angular momentum, $\vec{J}$, and has the same direction. If the electron is not considered a point charge, a more exact expression for $\vec{\mu}$ is:

$$\vec{\mu} = -\frac{ge}{2m}\vec{J} = -g\frac{e}{2m}\sqrt{J(J+1)}\frac{h}{2\pi} \qquad (A.1)$$

where g is the Landé factor whose magnitude is given by (Banwell 1983):

$$g = \frac{3}{2} + \frac{S(S+1) - L(L+1)}{2J(J+1)} \qquad (A.2)$$

Since $\vec{\mu}$ is proportional to $\vec{J}$, $\vec{\mu}$ will also have components in the z direction:

$$\mu_z = -\frac{ge}{2m}\frac{h}{2\pi}J_z \qquad (A.3)$$

If an external magnetic field is applied to the atom (thus specifying the previously arbitrary z direction), the atomic dipole $\vec{\mu}$ will interact with the applied field to an extent depending on its components in the field direction. If the strength of the applied field is B_z then the extent of the interaction is $\Delta E = \vec{\mu}B_z$ (Woodgate 1980):

$$\Delta E = \mu_z B_z = -\frac{heg}{4\pi m}B_z \qquad (A.4)$$

Equation (A.4) expressed in terms of the frequency difference $\Delta\nu$ (cm^{-1}) is:

$$\Delta\nu = 4.669 X 10^{-5} B m_j g_j \qquad (A.5)$$

where B is the magnetic field in gauss and g_j is the Lande g factor. The Zeeman displacements for Rb 6P atoms are listed in Table A.I and the splittings of the substates in B = 4.75T are drawn in Fig. A.1.

TABLE A.1

Zeeman Displacements $\Delta\nu$ (cm^{-1}) for B = 4.75 T.

FS State	g_J	m_J	$\Delta\nu(cm^{-1})$
$5^2S_{1/2}$	2	1/2	2.22
$6^2P_{1/2}$	2/3	1/2	0.739
$6^2P_{3/2}$	4/3	1/2	1.48
$6^2P_{3/2}$	4/3	3/2	4.44

Fig A.1 Relative displacements of the 6P Zeeman substates of rubidium for a magnetic field of 4.75 T (drawn to scale).

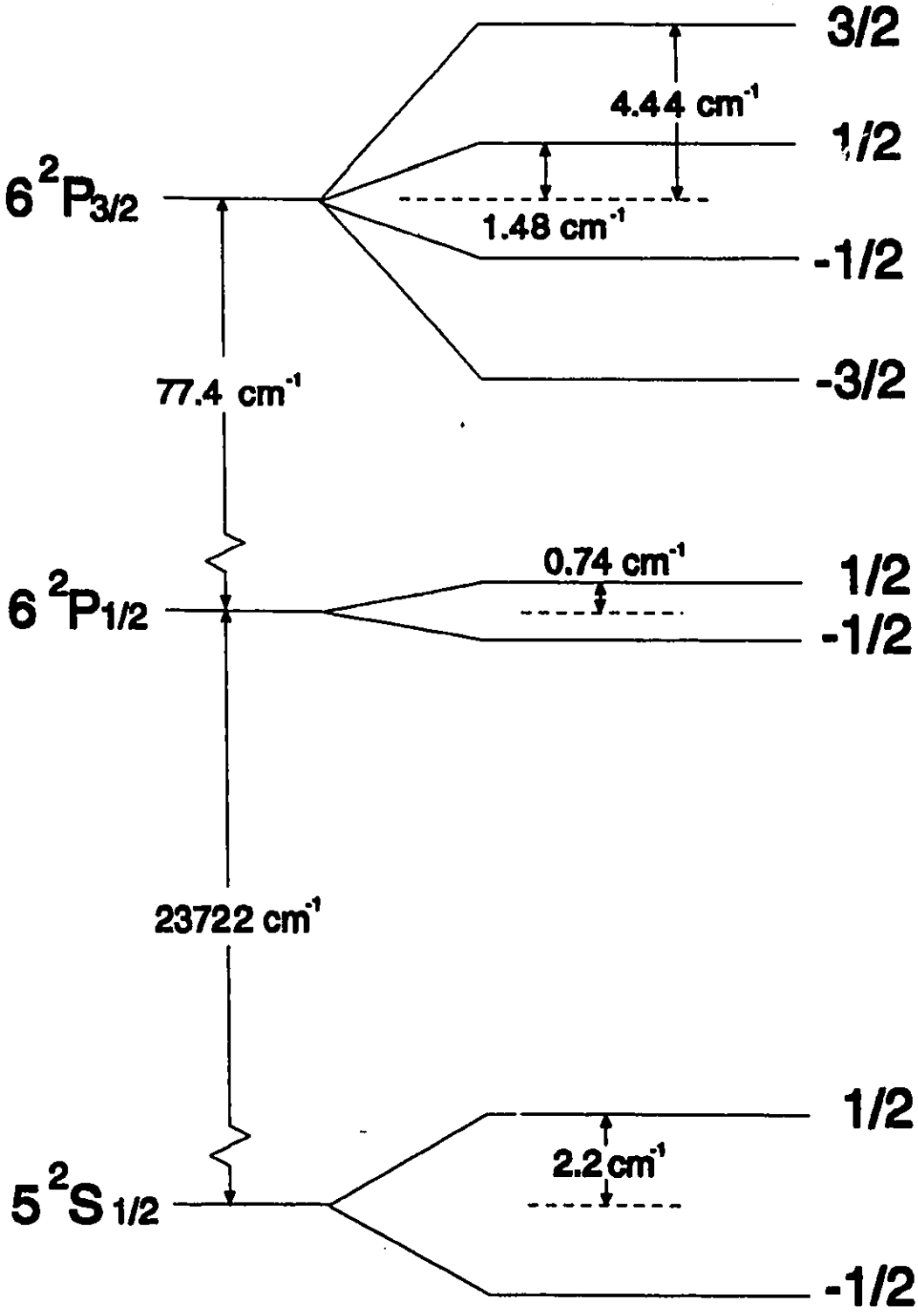
3/2
4.44 cm-1
1/2
6 2P3/2
1.48 cm-1
-1/2
-3/2
77.4 cm-1
0.74 cm-1
1/2
6 2P1/2
-1/2
23722 cm-1
1/2
2.2 cm-1
5 2S 1/2
-1/2

Vita Auctoris

I was born on March 26, 1963 in Lethbridge Alberta, graduated from the Lethbridge Collegiate Institute in 1981 and entered the University of Lethbridge the following year. In 1986, I received a B.A.Sc. degree in Physics from the University of Lethbridge. At present I am a candidate for the M.Sc. degree in Physics at the University of Windsor (Windsor, Ontario) and expect to graduate in June 1991.